D'Arcy, M., Mason, P. J., Roda-Boluda, D. C., Whittaker, A. C., Lewis, J. M. T., Najorka, J. (2018): Alluvial fan surface ages recorded by Landsat-8 imagery in Owens Valley, California. - *Remote Sensing of Environment*, *216*, pp. 401—414.

DOI: http://doi.org/10.1016/j.rse.2018.07.013

Alluvial fan surface ages recorded by Landsat-8 imagery in Owens Valley, California

Mitch D'Arcy[1,2]*; Philippa J. Mason[3]; Duna C. Roda-Boluda[2]; Alexander C. Whittaker[3]; James M.T. Lewis[3]; Jens Najorka[4]

[1]Institute of Earth and Environmental Science, University of Potsdam, Karl-Liebknecht-Straße 24-25, 14476 Potsdam-Golm, Germany

[2]Helmholtz Centre Potsdam, GFZ German Research Centre for Geosciences, Telegrafenberg, 14473 Potsdam, Germany

[3]Department of Earth Science and Engineering, Imperial College London, South Kensington Campus, Exhibition Road, London SW7 2AZ, United Kingdom

[4]Natural History Museum, Cromwell Road, London SW7 5BD, United Kingdom

*Corresponding author. Email: mdarcy@uni-potsdam.de; Phone: +49 331 2882 8832.

Abstract

Alluvial fans are important depositional landforms that offer valuable records of terrestrial sedimentation history if their surfaces can be mapped and dated accurately. Unfortunately, as this often depends on detailed field mapping and intensive absolute dating techniques, it can be a challenging, expensive and time-consuming exercise. In this study, we demonstrate that quantitative information about the ages of alluvial fan surfaces in Owens Valley, California, is recorded by Landsat-8 multispectral satellite imagery. We show that systematic changes in the wavelength-dependent brightness of fan surfaces occur gradually over a timescale of ~100 kyr in this semi-arid setting, and are highly correlated with known deposit ages. Using spectro-radiometry and X-ray diffraction analysis of sediment samples collected in the field, we

interpret that surface reflectance evolves primarily in response to the in-situ production of secondary illite and iron oxide by weathering in this landscape. Furthermore, we demonstrate that first-order predictions of absolute fan surface age can be derived from multispectral imagery when an initial age calibration is available. These findings suggest that multispectral imagery, such as Landsat data, can be used (i) for preliminary mapping of alluvial fans prior to detailed field work and before choosing sampling sites for conventional dating techniques, and (ii) to extend age models to un-dated neighbouring surfaces with equivalent physical properties, once an age-brightness calibration has been established.

1. Introduction

Alluvial fans are depositional landforms that occur in sedimentary basins worldwide and record useful information about landscape evolution and source-to-sink sedimentation (Armitage et al., 2011; Frankel et al., 2011; Hedrick et al., 2013; Owen et al., 2014; D'Arcy et al., 2017a). They typically comprise multiple superposed and juxtaposed surfaces that become abandoned and preserved as a result of incision, aggradation and/or avulsion (Harvey et al., 1999; D'Arcy et al., 2015). Dated alluvial fan surfaces therefore represent distinct time periods of deposition, and have been used as markers to infer fault slip rates and tectonics (e.g., Porat et al., 1997; Kirby et al., 2006; Frankel et al., 2007a, 2011), and examine how past climate changes have affected sedimentation (e.g., White et al., 1996; Owen et al., 2014; D'Arcy et al., 2017a,b). In order to make use of alluvial fans as sedimentary archives of information, techniques for precisely mapping and dating their surfaces are essential.

Today, approaches available for the absolute dating of fan surfaces include cosmogenic radionuclide exposure dating (Dühnforth et al., 2007; Frankel et al., 2007a; Machette et al., 2008), luminescence techniques (Sohn et al., 2007), radiocarbon dating (Reheis et al., 1993), and U-series dating of pedogenic carbonates (Blisniuk et al., 2012; Oerter et al., 2016), among others (Noller et al., 2000). Inevitably, these techniques need to be used in combination with

surface mapping for (i) selecting suitable sampling sites, and (ii) correlating and interpreting ages (Owen et al., 2011). In the field, fan surfaces can be mapped prior to absolute dating by using a variety of relative age indicators. These include soil development (Harden, 1987; Zehfuss et al., 2001), clast weathering (Bull, 1991; D'Arcy et al., 2015), surface roughness (Frankel & Dolan, 2007; Regmi et al., 2014), rock varnish and desert pavement maturity (Bull, 1991; Wells et al., 1995), soil carbonate content (Machette, 1985), fault scarp offsets (Le et al., 2007), sedimentological properties such as grain size (Al-Farraj & Harvey, 2000; D'Arcy et al., 2017a,b), and surface morphology (Beratan & Anderson, 1998). These age indicators are most powerful when used in combination with each other and with absolute dating efforts (McFadden et al., 1989; D'Arcy et al., 2015).

Remote sensing is another valuable tool for mapping and correlating geomorphic features such as alluvial fan surfaces. It has long been recognised that fan surfaces of different age can be discriminated using multispectral imagery (Gillespie et al., 1984; Kahle et al., 1984; Gillespie, 1992). Differences in the reflectance properties of fan surfaces with different ages have been attributed to changes in chemistry, mineralogical composition and micro-relief as a result of sustained weathering (Gillespie et al., 1984; Kahle et al., 1984; Farr, 1985; Bull, 1991), and specific minerals can be identified within alluvial fan deposits from their reflectance spectra (Shipman & Adams, 1987; Ferrier & Pope, 2012). The gradual accumulation of brown-black rock varnish on clasts and red-brown clays in soils and desert pavements also darkens fan surfaces over time and reduces their albedo in many arid landscapes (Hunt & Mabey, 1966; Bull, 1991; Stock et al., 2007). More recently, it has been suggested that multispectral and hyperspectral imagery can be used to derive information about the types of sedimentary deposits present on alluvial fan surfaces (Milana, 2000; Crouvi et al., 2006; Hardgrove et al., 2010), and that the relationship between fan surface age and brightness is quantifiable (Dickerson et al., 2015). Ground-based studies have also shown that desert pavements act to polarize sunlight (Hibbitts & Gillespie, 2008), and average radar backscatter as a roughness proxy has been shown to correlate with the ages of alluvial surfaces in Israel and Jordan (Hetz

et al., 2016). However, despite freely-available multispectral satellite imagery and a rapidly increasing number of published alluvial fan chronologies, the opportunity for mapping fan surfaces and predicting their ages using remotely-sensed data remains significantly under-explored. In this study, we use Landsat-8 imagery to characterise the visible to shortwave infrared (0.4-2.5 μm) spectral properties of 33 distinct alluvial fan surfaces in Owens Valley, California, which have depositional ages spanning the last ~125 kyr. Over this timespan we identify systematic changes in spectral character—i.e., brightness changes across the visible and near infra-red (VNIR) and short-wave infra-red (SWIR) spectral bands—that correlate with independently-obtained absolute fan surface ages. By comparing areas burned in wildfires with unburned parts of the fan surfaces, we show that age-related changes in surface brightness are largely insensitive to vegetation density. We then investigate the origins of these spectral patterns using both XRD and laboratory spectro-radiometry, and explore the opportunity presented for remote mapping of alluvial fans and developing preliminary surface age models. Building upon previous studies that distinguish relative fan surface ages using multispectral/thermal imagery (Gillespie et al., 1984; Kahle, 1987; Hardgrove et al., 2010) and radar (Farr and Chadwick, 1996), we demonstrate that it is also possible to distinguish between fan surfaces of different ages using Landsat-8 imagery, at least in Owens Valley. Finally, we perform a comparison between our target fan surfaces in Owens Valley and additional fan surfaces in neighbouring Death Valley, California.

2. Study Area

We examine eight alluvial fan sequences in Owens Valley, California (Fig. 1). These fans comprise debris flow deposits exported by steep catchments along the eastern Sierra Nevada (cf. D'Arcy et al., 2015). The deposits are exclusively granitic in composition, owing to the constant bedrock lithology in the parent catchments; detailed lithological descriptions are provided by Bateman (1992). They have been mapped and dated by previous studies with a

combined total of 89 ^{10}Be cosmogenic nuclide exposure dates spanning >100 kyr (Zehfuss et al., 2001; Dühnforth et al., 2007; Le et al., 2007). D'Arcy et al. (2015, 2017b) subsequently combined and updated these ^{10}Be ages using a refined estimate of boulder surface lowering rate, consistent parameters for the age calculations, and information about the timing of past glaciation from the Birch Creek fan. D'Arcy et al. (2015) also extended the ^{10}Be age model to neighbouring fan surfaces by developing an empirical correlation technique based on the weathering rate of boulders. With 33 dated surfaces, these fans have an exceptional density of age constraints across time and space, and we refer the reader to D'Arcy et al. (2015, 2017b) for full mapping and dating information. Therefore, the Owens Valley fans present a particularly well-constrained opportunity to characterise how surface reflectance evolves over 10^4 to 10^5 year timescales in a semi-arid environment.

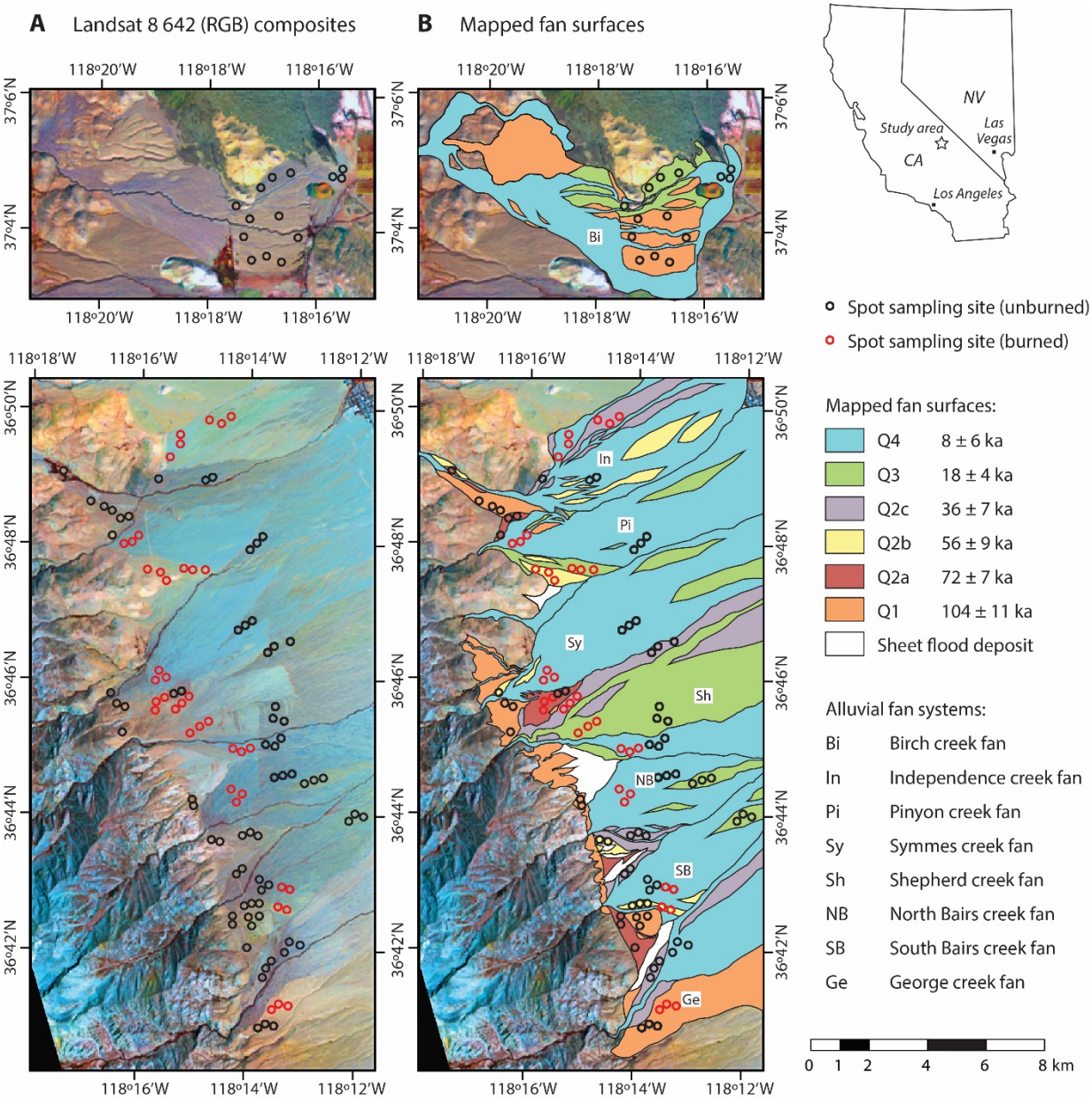

Fig. 1. Maps locating the target fan surfaces in Owens Valley, California. (A) Landsat-8 false colour composite (642 RGB, date: 12th May 2013) showing spot sampling sites (unburned fan surfaces in black, burned surfaces in red). (B) Corresponding fan surface maps and ages are taken from D'Arcy et al. (2015). Younger surfaces appear more blue and older surfaces appear more orange.

Owens Valley is a semi-arid basin occupying the rain shadow of the Sierra Nevada. Modern mean annual precipitation averages 50-200 mm yr^{-1} and annual temperatures average 14-18 °C (2004-2013 records from Independence; NOAA National Climatic Data Center, 2014). The climate was colder and wetter on average during the glacial period of the late Pleistocene; the Last Glacial Maximum (LGM) was 5-6 °C cooler and approximately twice as wet as modern conditions (e.g., Benson et al., 1996; Woolfenden, 2003; Yamamoto et al., 2007; Phillips, 2008).

Today, vegetation on the alluvial fans is limited to sparse cover of semi-arid shrub communities (Fig. 2; Ustin et al., 1986; Smith et al., 1990a,b). After ~100 kyr of exposure the fan surfaces are discoloured and remain mantled by alluvial sediment (Fig. 2b). Detailed soil descriptions are provided by Zehfuss et al. (2001), which we supplement with XRD and spectro-radiometry analyses in this study. In places, wildfires have occurred on small patches of the fan surfaces, which appear brighter in imagery (Fig. 1) as a result of a reduction in vegetation density from 45-55% cover (mature, unburned surfaces) to 15-25% cover (recently burned surfaces). These measurements of vegetation coverage were obtained by thresholding high-resolution (<1 m per pixel) aerial imagery of the fan surfaces, in which vegetation appears dark and sediment appears light, and counting the number of pixels that correspond to vegetation. Following several wildfires on these fan surfaces, it has been observed that the resulting charcoal is removed by wind (Bierman and Gillespie, 1991). We take advantage of these burned patches of fan surfaces to evaluate what effect a significant (~30%) reduction in vegetation cover has on the spectral characteristics of our target alluvial fan surfaces.

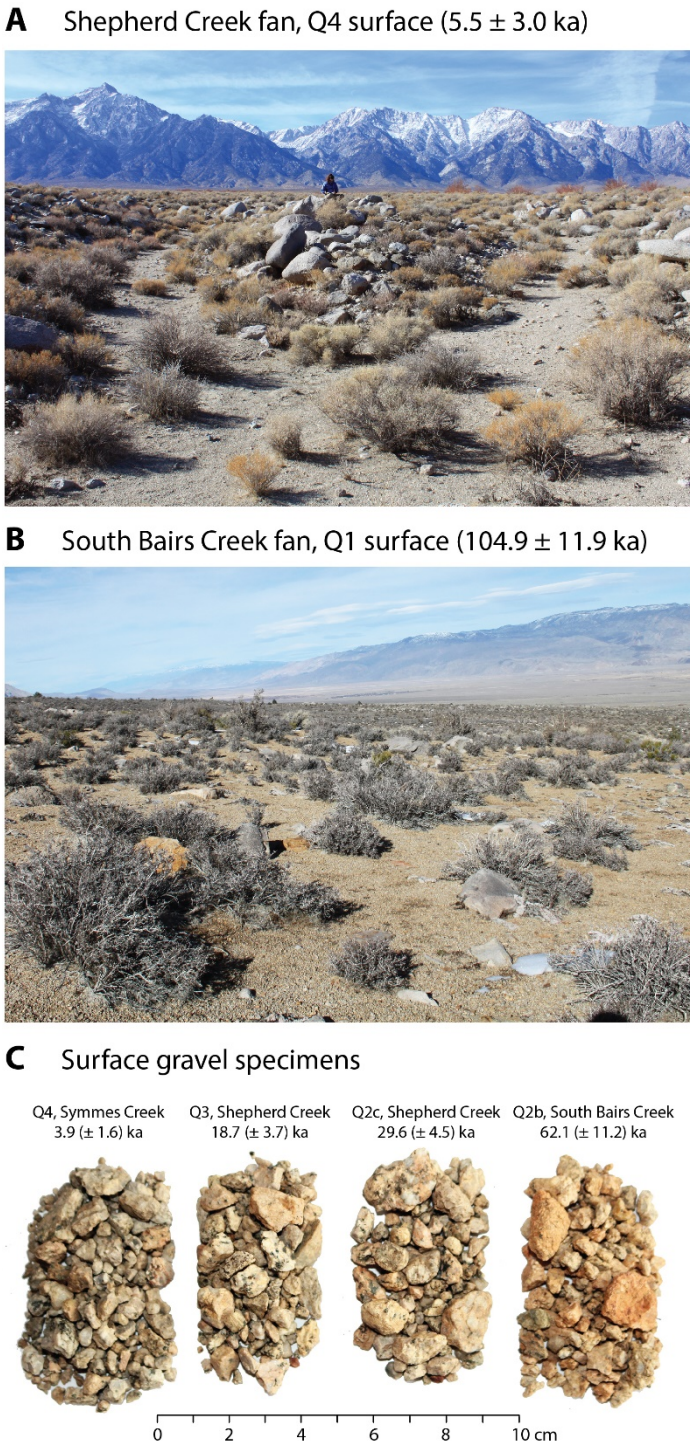

Fig. 2. Field photographs of (A) a Q4 surface and (B) a Q1 surface taken in sunny conditions with constant camera settings and no contrast enhancement. These photographs show mature vegetation on these fans (unburned surfaces), which is dominated by sparse coverage of semi-arid shrubs (Ustin, 1986; Smith et al. 1990a). Sediment colour turns from grey to

yellow with age and boulders become slightly varnished. (C) The change in colour can also be seen in gravel samples taken from various surfaces and photographed under constant lighting conditions. Ages are taken from D'Arcy et al. (2015).

Even without the age constraints provided by previous studies, younger and older surfaces are easily discriminated in the field. Figure 2 shows field photographs of two fan surfaces, one dating to ~5.5 ka and the other to >100 ka. These pictures were taken in November 2013 with the same camera settings and constant white balance, in equivalent sunny lighting conditions and with no subsequent contrast enhancement; they therefore give a fair comparison of surface appearance. The younger surface (Fig. 2a) shows a debris flow snout with white-grey boulders surrounded by a pale grey gravel surface. The original depositional relief is intact and the clasts are bright, unweathered and unvarnished. By contrast, the older surface (Fig. 2b) exhibits weathered boulders with a moderate amount of dark grey varnishing on their top surfaces. The original depositional relief has degraded by diffusion, and the gravels and some of the boulder clasts have become orange as a result of oxidation. These post-depositional changes take place gradually. Figure 2c shows photos of surface gravels (~10 mm) collected from surfaces spanning 4 to 62 ka. These images were also taken with constant lighting and camera settings/white balance, and no contrast enhancement was applied. They illustrate the intensity of the change in sediment colour over several 10s of kyr, which is apparent both in the field and in hand specimens.

3. Methods

We downloaded multispectral imagery for two cloud-free Landsat 8 scenes covering our target alluvial fans (path 41/row 35 and path 42/row 34), imaged on 12th May 2013. We selected Landsat 8 imagery for this study because it is freely available globally and widely-used, has a 30 m pixel resolution, and offers good spectral resolution with 7 bands between 0.43 and 2.29

μm wavelength. For each band, both scenes were combined to form a single raster, which was then clipped to a smaller study box covering only the alluvial fans (with corners situated at 37.097N, 118.464W; 37.152N, 118.242W; 36.537N, 118.251W; and 36.601N, 118.026W). The image data were first converted to an 8 bit value range using a simple linear transform. We then applied the Balanced Contrast Enhancement Technique (BCET) (Liu, 1991), which stretches the histogram of each spectral band to the same mean (110) and value range (exactly between 0 and 255) using a parabolic function without modifying its fundamental shape and, importantly, without distorting the spectral information. The BCET technique is commonly used to perform contrast enhancement prior to colour composite construction, in order to remove colour bias and ensure a fair comparison between spectral bands (Liu and Mason, 2016). The bands of any multispectral sensor are normally very highly correlated and require correction to examine the true spectral differences between different target minerals. Therefore, the BCET stretch also effectively cancels out the common information among the bands, leaving the spectrally-unique information that characterises different ground materials, e.g., rocks, soils, minerals, vegetation. As we are interested in characterising these relative spectral differences, rather than identifying the materials, we selected BCET instead of attempting to correct imagery to surface reflectance by atmospheric corrections. We refer the reader to Liu & Mason (2016) for a thorough explanation of the BCET technique.

Subsequently, we used a 'spot' sampling approach to measure the reflectance of each fan surface. Sampling spots with surface diameters of 200 m (averaging 35 pixels of Landsat 8 imagery) were placed on representative parts of the fan surfaces (Fig. 1), and the zonal statistics tool in ArcGIS v10.3 was used to extract the mean pixel value in each spot, for each band. We used 3 spots to characterise each surface (apart from 6 small fan surfaces that were only large enough for 1 or 2 spots; see Fig. 1 and supplementary information), and took averages of these triplicate measurements. Spot sampling is an effective strategy for characterising surfaces in multispectral imagery (e.g., Dickerson et al., 2015), allowing us to (i) perform repeat measurements; (ii) target stable and well-exposed parts of fan surfaces at

locations where age constraints were collected by previous workers; and (iii) deliberately avoid unwanted features like vegetated streams and gullies, bedrock mounds, resurfaced paths, and agriculture. All dated surfaces were spot-sampled at 'unburned' locations with mature coverage of semi-arid shrubland (see Fig. 2 for representative field photographs). For 14 of the surfaces, it was also possible for us to spot-sample 'burned' locations of the fan surfaces that have experienced wildfires (Fig. 1); these burn scars exhibit ~30% reduced vegetation density and allow us to investigate the role vegetation coverage plays in modulating the spectral properties of the fan surfaces. In addition to sampling each individual fan surface, we also averaged the data for each stratigraphic unit across all 8 fan systems (with surfaces weighted equally). These stratigraphic averages offer the major advantage of binning multiple fan surfaces of equivalent age to increase the signal/noise ratio.

We also collected visible and near infrared (VNIR) and short-wave infrared (SWIR) reflectance spectra, under dark laboratory conditions, for 4 sediment samples collected in the field, each from a different fan surface. These samples comprised a mixture of gravel (1-15 mm particle diameters) and finer material collected from the uppermost fan surfaces (no buried/subsurface material was included) on stable parts of the fans well away from any streams, incision or re-working. We targeted the Q4 (Symmes creek fan), Q3 (Shepherd creek fan), Q2c (Shepherd creek fan) and Q2b (South Bairs creek fan) surfaces because these have a variety of ages (Fig. 1). The samples were scanned in a dark laboratory using an ASD TerraSpec 4 portable spectro-radiometer, with a Hi-Brite Contact Probe that provides a direct, spectrally-uniform illumination source and collects reflected light. For each sample, average spectra were created using 3 scans at slightly different points over a 1 cm window to ensure strong and reliable spectra. The spectra were then analysed using The Spectral Geologist (TSG) and The Spectral Assistant (TSA) software, which adopt a matching algorithm to identify spectra as linear mixtures of library mineral spectra to find a best match spectrum. Independent analysis of the spectra was also undertaken by ASD Inc. (PANalytical) utilising the Halo mineral

identifier. The considerably larger library of mineral spectra that Halo incorporates enabled the identification of additional minerals that TSG and TSA could not.

For two of these samples (Q4 and Q2b), we also performed X-ray diffraction (XRD) analyses on the clay fractions in order to identify any changes in composition over a period of ~60 kyr. Each sample was mixed with distilled water and centrifuged for four minutes at 1000 rpm to separate the clay fraction from the bulk material. The clay-containing supernatant was decanted and centrifuged for 20 minutes at 4000 rpm. The water was decanted but a small amount retained to re-suspend the clay. The clay suspensions were then added drop wise to glass slides and dried on a hot plate at 50 °C. The XRD analyses were performed with a Panalytical X'Pert Pro Alpha-1 system. Each clay fraction was analysed between 2 and 40 °2θ for 5 hours and 15 minutes using copper radiation with an X'Celerator detector. Tube operation conditions were 45 KV and 40 mA. The Panalytical Highscore software package was used in combination with the ICDD PDF-2 database to identify the mineral phases.

4. Results

4.1. Fan surface brightness in Landsat 8 imagery

Figure 3 shows the average BCET-corrected image brightness in each Landsat-8 band from 1 (0.43-0.45 μm) to 7 (2.11-2.29 μm), for a series of sample locations that are spatially-distributed across each stratigraphic unit and all fan systems (see Fig. 1 for spot locations, and Tables 1 and 2 for original data). Burned and unburned surfaces are shown in red and black, respectively. Coloured shading shows ±1 σ variability in values between individual sampling spots for each unit. Burned surfaces are slightly brighter than unburned surfaces, and in some instances the burned surfaces are very slightly brighter in red light (band 4), owing to the enhanced surface coverage of bare, orange-coloured surface sediment (Fig. 2). Otherwise, the relative patterns between spectral bands are equivalent for burned and unburned surfaces. There is no significant variation in overall brightness between older and

younger surfaces, which have consistent BCET digital number values ranging between 100 and 160. However, there are significant temporal differences in the pattern of relative brightness across the spectral bands. The youngest surfaces (Fig. 3a) are brightest in VNIR bands 1 and 2, at the shortest wavelengths.

As surface age increases, peak brightness shifts towards progressively longer wavelengths in the SWIR bands such that by 20-35 ka (Fig. 3b-c) the spectral profile is relatively flat, and for older surfaces the peak brightness lies in the SWIR around band 6. There is a systematic reversal of the overall slope of these BCET spectral profiles from negative (Q4) to positive (Q1) over time. Relative brightness in the visible wavelengths decreases and peak brightness shifts from shorter to longer wavelengths as recorded by Landsat 8 bands 1-7, over a period of ~100 kyr. In Fig. 4, this effect is illustrated by normalising each average spectral band value from the profiles in Fig. 3 using the band 2 average value. The youngest fan surfaces reflect most strongly in shorter wavelength (VNIR bands), but as they age they become systematically less reflective in the VNIR bands, so that relative SWIR brightness becomes progressively stronger, peaking in band 6. The spectral properties of these dated surfaces are therefore sensitive to their known ages, at least over the last 100 kyr.

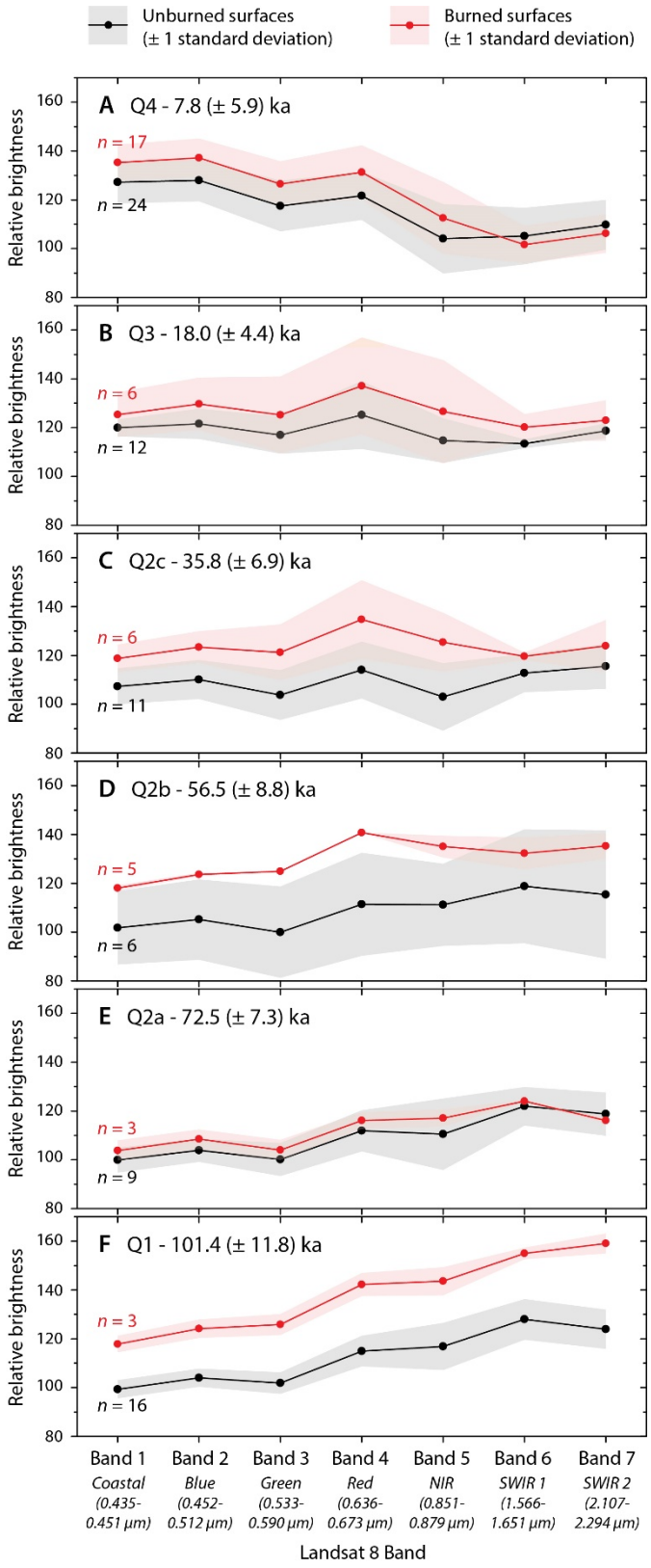

Fig. 3. Average BCET spectral profiles (Landsat 8 bands 1-7) for each stratigraphic fan unit, showing the relative brightness at spot-sampled locations. Data are shown as the BCET relative brightness, i.e. represented as a value between 0 and 255. Solid lines show mean

brightness for each stratigraphic unit, averaged across all fans (*n* gives the number of spot locations). Shading shows ±1 σ variability between all sampling spots. As surfaces get older, peak brightness shifts to SWIR bands (longer wavelengths), and this is observed for burned and unburned surfaces.

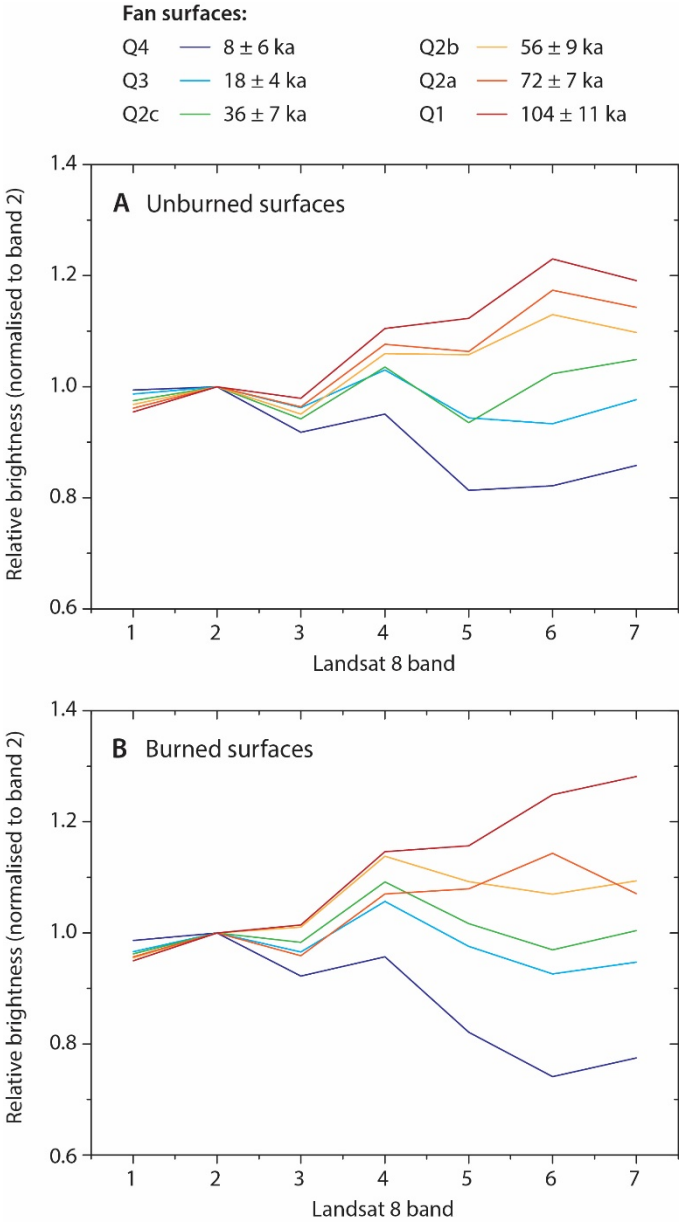

Fig. 4. Average spectral profiles from Fig. 3 for (A) unburned fan surfaces and (B) burned fan surfaces, normalised to band 2 (blue light). Relative brightness in bands 3-7 increases with surface age, with band 6 showing the greatest sensitivity.

					Average BCET brightness																	
Alluvial fan system	Surface	Age (ka)	± (ka)	No. sampling spots	B1	±	B2	±	B3	±	B4	±	B5	±	B6	±	B7	±	B6/B2 ratio	±		
Unburned alluvial fan surfaces																						
Symmes	Q4	3.9	1.6	3	129.2	*2.2*	130.9	*1.8*	119.7	*1.2*	126.1	*0.8*	109.3	*1.0*	102.5	*1.4*	105.2	*2.0*	0.78	*0.02*		
Shepherd	Q4	5.5	3.0	3	133.6	*1.9*	135.5	*1.4*	124.2	*1.3*	128.4	*1.5*	107.7	*2.5*	104.1	*3.6*	111.5	*3.3*	0.77	*0.03*		
South Bairs	Q4	5.6	2.4	3	110.8	*2.6*	111.7	*2.5*	100.5	*2.7*	106.0	*2.4*	85.8	*1.7*	97.4	*1.4*	101.3	*1.2*	0.87	*0.03*		
North Bairs	Q4	6.7	5.7	3	129.1	*3.8*	129.6	*3.8*	116.4	*3.5*	119.6	*3.3*	98.0	*3.4*	95.6	*1.3*	102.1	*1.9*	0.74	*0.03*		
Pinyon	Q4	7.5	3.4	3	131.3	*2.8*	134.2	*3.0*	125.7	*3.1*	132.0	*2.9*	115.0	*3.2*	108.7	*1.1*	110.9	*1.0*	0.81	*0.03*		
Birch	Q4	8.5	2.1	3	139.1	*1.5*	137.2	*1.9*	132.8	*1.3*	132.8	*0.7*	129.7	*0.2*	131.9	*2.3*	133.1	*2.2*	0.96	*0.03*		
George	Q4	11.9	5.1	3	122.5	*13.8*	122.0	*14.9*	107.7	*15.5*	111.0	*15.4*	92.3	*14.6*	102.2	*6.7*	109.7	*8.7*	0.84	*0.18*		
Independence	Q4	13.1	4.6	3	122.1	*4.7*	122.9	*5.1*	112.8	*6.9*	117.6	*6.4*	94.8	*4.6*	98.9	*1.3*	104.8	*2.8*	0.80	*0.05*		
Birch	Q3	14.1	1.7	3	115.8	*1.5*	112.7	*1.4*	106.8	*1.3*	105.8	*1.4*	103.2	*1.1*	113.8	*1.6*	115.5	*2.2*	1.01	*0.03*		
North Bairs	Q3	18.0	7.9	3	118.5	*1.6*	122.0	*1.4*	119.5	*1.9*	132.8	*1.8*	121.3	*1.6*	114.2	*0.6*	120.0	*1.0*	0.94	*0.02*		
South Bairs	Q3	18.0	7.9	3	122.3	*0.7*	126.5	*0.6*	124.9	*0.9*	137.4	*1.4*	122.8	*2.1*	115.0	*1.4*	122.4	*1.5*	0.91	*0.02*		
Shepherd	Q3	18.7	3.7	3	123.2	*2.7*	125.0	*3.1*	116.6	*3.2*	124.9	*3.4*	111.6	*3.2*	110.8	*3.4*	117.0	*3.6*	0.89	*0.05*		
Shepherd	Q2c	29.6	4.5	3	112.8	*1.2*	115.3	*1.3*	110.6	*1.7*	122.5	*1.9*	112.7	*1.0*	111.7	*0.9*	116.7	*1.1*	0.97	*0.02*		
George	Q2c	35.2	13.2	3	105.7	*1.5*	107.1	*1.4*	96.4	*1.4*	103.6	*1.9*	88.6	*2.2*	103.7	*0.3*	106.9	*0.2*	0.97	*0.02*		
North Bairs	Q2c	36.4	9.4	3	113.2	*0.8*	117.9	*0.8*	114.4	*1.1*	125.6	*1.8*	116.7	*5.5*	122.8	*4.6*	127.9	*3.3*	1.04	*0.05*		
South Bairs	Q2c	37.4	13.5	2	97.7	*3.9*	100.3	*4.2*	93.7	*5.1*	104.5	*5.5*	94.0	*6.2*	112.8	*3.8*	110.7	*3.7*	1.12	*0.09*		
North Bairs	Q2b	56.5	20.8	2	115.0	*1.7*	119.4	*1.8*	115.0	*2.8*	127.2	*3.5*	127.2	*1.6*	140.9	*5.7*	138.1	*6.5*	1.18	*0.07*		
Symmes	Q2b	56.5	6.9	1	85.4	*4.3*	87.2	*5.6*	79.1	*7.6*	87.5	*8.8*	93.6	*10.9*	94.4	*8.6*	86.5	*9.1*	1.08	*0.18*		
South Bairs	Q2b	62.1	11.2	3	104.9	*3.0*	108.9	*3.1*	105.8	*4.7*	119.4	*6.0*	112.7	*7.1*	121.0	*2.1*	121.5	*3.1*	1.11	*0.05*		
Shepherd	Q2a	68.2	7.5	2	100.9	*1.5*	103.1	*1.9*	95.2	*3.4*	105.3	*4.7*	94.4	*6.3*	116.0	*6.0*	115.8	*6.6*	1.13	*0.08*		
Pinyon	Q2a	70.3	8.1	3	106.1	*3.1*	110.7	*3.5*	110.0	*5.1*	124.0	*7.4*	117.1	*10.9*	129.5	*8.9*	131.5	*8.6*	1.17	*0.12*		
South Bairs	Q2a	72.5	14.6	3	98.8	*2.6*	102.1	*2.4*	96.5	*1.7*	107.2	*1.9*	103.1	*5.3*	114.4	*2.2*	111.0	*1.5*	1.12	*0.05*		
Independence	Q2a	79.0	7.4	1	93.8	*7.4*	99.9	*8.5*	98.8	*8.5*	111.0	*11.0*	127.4	*6.6*	127.9	*8.1*	116.7	*9.5*	1.28	*0.21*		
Independence	Q1	90.9	18.1	3	101.0	*1.0*	104.4	*1.1*	99.5	*0.8*	110.0	*1.4*	98.0	*2.2*	115.4	*2.0*	116.4	*0.7*	1.11	*0.03*		
George	Q1	97.4	14.9	3	101.4	*3.7*	106.0	*4.2*	103.5	*4.1*	118.6	*4.7*	116.6	*2.0*	140.8	*1.0*	139.3	*2.7*	1.33	*0.06*		
Symmes	Q1	104.1	35.1	2	95.6	*3.8*	101.0	*4.4*	98.6	*4.3*	111.3	*5.2*	119.7	*3.4*	131.3	*8.2*	121.4	*5.9*	1.30	*0.14*		
Shepherd	Q1	104.1	35.1	3	100.7	*15.4*	106.6	*17.8*	103.7	*20.9*	114.1	*22.2*	124.1	*20.5*	129.0	*20.1*	123.1	*22.9*	1.21	*0.47*		
South Bairs	Q1	104.1	35.1	3	103.4	*2.7*	108.1	*2.6*	108.9	*3.8*	125.8	*4.9*	120.0	*2.9*	125.2	*3.0*	124.5	*1.0*	1.16	*0.06*		
North Bairs	Q1	104.9	11.9	2	93.8	*2.9*	98.3	*2.9*	96.9	*2.8*	109.8	*1.1*	122.8	*2.6*	126.2	*1.7*	118.9	*3.1*	1.28	*0.06*		
Birch	Q1	122.5	14.5	8	112.5	*3.6*	111.8	*3.5*	112.5	*3.0*	118.9	*2.0*	119.5	*2.8*	141.7	*2.8*	146.6	*2.8*	1.27	*0.07*		
Burned alluvial fan surfaces																						
Symmes	Q4	3.9	1.6	3	138.1	*2.8*	139.5	*2.6*	126.3	*2.1*	129.7	*1.8*	112.8	*1.5*	100.8	*1.4*	102.8	*1.6*	0.72	*0.02*		
Shepherd	Q4	5.5	3.0	3	143.2	*3.3*	144.6	*3.3*	132.2	*3.5*	134.9	*3.9*	114.1	*3.3*	102.1	*1.7*	108.1	*2.9*	0.71	*0.03*		
South Bairs	Q4	5.6	2.4	2	125.7	*2.7*	127.8	*2.6*	119.2	*2.9*	124.7	*3.0*	101.4	*2.4*	99.1	*1.0*	106.7	*1.5*	0.78	*0.02*		
North Bairs	Q4	6.7	5.7	3	128.7	*2.4*	129.3	*2.7*	115.8	*2.9*	118.9	*2.8*	101.5	*3.0*	94.1	*2.1*	96.8	*2.3*	0.73	*0.03*		
Pinyon	Q4	7.5	3.4	3	132.8	*3.1*	134.7	*3.1*	124.0	*2.8*	128.3	*2.4*	105.4	*0.8*	97.8	*0.6*	103.0	*1.0*	0.73	*0.02*		
Independence	Q4	13.1	4.6	3	143.1	*3.2*	147.2	*3.3*	141.7	*3.9*	151.2	*4.3*	140.7	*3.4*	116.2	*2.5*	120.4	*3.1*	0.79	*0.04*		
Shepherd	Q3	18.7	3.7	3	118.9	*6.9*	122.1	*7.2*	114.2	*6.9*	123.1	*6.8*	111.6	*6.5*	116.4	*1.2*	117.0	*2.3*	0.95	*0.07*		
Pinyon	Q3	21.2	4.3	3	131.8	*3.0*	137.4	*3.1*	136.3	*4.0*	151.1	*4.6*	141.5	*3.9*	124.0	*3.1*	128.8	*4.2*	0.90	*0.04*		
Shepherd	Q2c	29.6	4.5	3	114.7	*4.2*	118.8	*3.4*	113.2	*2.2*	123.3	*1.8*	117.0	*2.4*	120.7	*5.1*	116.4	*2.3*	1.02	*0.07*		
Independence	Q2c	40.2	10.4	3	122.8	*0.6*	128.1	*0.9*	129.3	*1.2*	146.1	*1.4*	134.0	*1.3*	118.5	*2.0*	131.4	*1.0*	0.93	*0.02*		
Pinyon	Q2b	48.6	12.0	3	117.3	*4.1*	123.2	*5.2*	124.9	*6.0*	140.7	*6.2*	138.1	*5.1*	136.9	*4.3*	139.0	*5.7*	1.11	*0.08*		
South Bairs	Q2b	62.1	11.2	2	118.9	*0.2*	124.1	*1.1*	125.0	*2.5*	140.8	*3.8*	131.9	*6.8*	127.6	*4.2*	131.5	*3.4*	1.03	*0.04*		
Shepherd	Q2a	68.2	7.5	3	103.8	*4.1*	108.5	*3.9*	104.0	*4.1*	116.1	*3.5*	117.1	*3.6*	124.0	*0.6*	116.1	*1.3*	1.14	*0.05*		
George	Q1	97.4	14.9	3	117.8	*3.4*	124.1	*3.7*	125.9	*4.3*	142.2	*4.8*	143.6	*5.7*	155.0	*2.4*	159.1	*4.0*	1.25	*0.06*		

Table 1. Average BCET brightness for each individual alluvial fan surface (sampled in burned and unburned locations), as measured using Landsat-8 imagery (see Methods for details). Surfaces ages are taken from D'Arcy et al. (2015).

					Average BCET brightness																	
Alluvial fan system	Surface	Age (ka)	± (ka)	No. sampling spots	B1	±	B2	±	B3	±	B4	±	B5	±	B6	±	B7	±	B6/B2 ratio	±		
Unburned alluvial fan surfaces																						
All fans	Q4	7.8	5.9	24	127.2	*8.7*	128.0	*8.6*	117.5	*10.4*	121.7	*9.8*	104.1	*14.2*	105.2	*11.6*	109.8	*10.2*	0.82	*0.16*		
All fans	Q3	18.0	4.4	12	119.9	*3.4*	121.6	*6.2*	116.9	*7.6*	125.2	*13.9*	114.7	*9.1*	113.4	*1.8*	118.7	*3.1*	0.93	*0.07*		
All fans	Q2c	35.8	6.9	11	107.4	*7.3*	110.2	*8.0*	103.8	*10.2*	114.0	*11.6*	103.0	*13.8*	112.8	*7.8*	115.5	*9.1*	1.02	*0.16*		
All fans	Q2b	56.5	8.8	6	101.8	*15.0*	105.2	*16.4*	100.0	*18.7*	111.4	*21.1*	111.2	*16.9*	118.8	*23.3*	115.4	*26.3*	1.13	*0.47*		
All fans	Q2a	72.5	7.3	9	99.9	*5.1*	103.9	*4.7*	100.1	*6.8*	111.9	*8.4*	110.5	*14.6*	122.0	*7.9*	118.8	*8.8*	1.17	*0.13*		
All fans	Q1	101.4	11.8	16	99.3	*3.7*	104.1	*3.7*	101.9	*4.4*	114.9	*6.3*	116.9	*9.6*	128.0	*8.3*	123.9	*8.1*	1.23	*0.13*		
Birch	Q1	122.5	14.5	8	112.5	*3.6*	111.8	*3.5*	112.5	*3.0*	118.9	*2.0*	119.5	*2.8*	141.7	*2.8*	146.6	*2.8*	1.27	*0.07*		
Burned alluvial fan surfaces																						
All fans	Q4	7.8	5.9	17	135.3	*7.4*	137.2	*8.0*	126.5	*9.3*	131.3	*11.1*	112.6	*14.8*	101.7	*7.6*	106.3	*7.9*	0.74	*0.10*		
All fans	Q3	18.0	4.4	6	125.3	*9.2*	129.8	*10.8*	125.3	*15.7*	137.1	*19.8*	126.6	*21.2*	120.2	*5.4*	122.9	*8.3*	0.93	*0.13*		
All fans	Q2c	35.8	6.9	6	118.7	*5.7*	123.4	*6.6*	121.3	*11.4*	134.7	*16.1*	125.5	*12.0*	119.6	*1.6*	123.9	*10.6*	0.97	*0.07*		
All fans	Q2b	56.5	8.8	5	118.1	*1.1*	123.6	*0.7*	124.9	*0.1*	140.7	*0.1*	135.0	*4.4*	132.2	*6.5*	135.2	*5.3*	1.07	*0.06*		
All fans	Q2a	72.5	7.3	3	103.8	-	108.5	-	104.0	-	116.1	-	117.1	-	124.0	-	116.1	-	1.14	-		
All fans	Q1	101.4	11.8	3	117.8	-	124.1	-	125.9	-	142.2	-	143.6	-	155.0	-	159.1	-	1.25	-		

Table 2. Average BCET brightness averaged for each stratigraphic unit across all fan systems (for burned and unburned sampling locations), as measured using Landsat-8 imagery. The average ages of the stratigraphic units are taken from D'Arcy et al. (2015).

Band 6 (1.57-1.65 μm; SWIR 1) shows the largest relative variation, meaning a ratio of brightness in band 6 divided by brightness in band 2 has the greatest age sensitivity in this particular dataset. The overall relative increase in the brightness of band 6 is ~40 % over a period of 100 kyr. In addition, Fig. 4 shows that bands 6 and 2 are sensitive to surface age for both unburned and burned fan surfaces. In Fig. 5, we plot this band 6/band 2 brightness ratio against fan surface age using linear (a) and logged (b) axes. The ratio is calculated for individual fan surfaces (open circles) and for stratigraphic averages that bin together all fan systems (black stars), and burned and unburned surfaces are plotted in red and black, respectively. For the stratigraphic averages, we separated the Q1 surface on the Birch creek fan because it is ~20 kyr older than the other Q1 surfaces and sufficiently older to be plotted separately. The brightness ratio increases sub-linearly from approximately 0.8 (Q4) to around 1.25 (Q1) over a period of ~120 kyr. A power law represents the stratigraphic averages very well (R^2 = 0.96-0.99), giving a starting ratio of ~0.6 for unburned surfaces and ~0.5 for burned surfaces when age = 0 and an exponent of 0.16 (standard error ±0.01) for unburned surfaces and 0.19 (±0.02) for burned surfaces. In other words, a reduction in vegetation cover in the burned zones acts to reduce the band 6/band 2 ratio by a small amount, but the rate and pattern of change with surface age is not significantly different compared to unburned fan surfaces. We chose to fit regressions to the stratigraphic averages because these obviously have the highest signal/noise ratio (see Methods), however if a power law is fitted to the individual fan surfaces R^2 is still high (0.86 for unburned surfaces and 0.90 for burned surfaces) and the parameters of the regression are the same as for the stratigraphic averages. As shown by Fig. 5b, this relationship therefore appears linear when the axes are logged, and has the greatest sensitivity to age in the 10-100 ka age range.

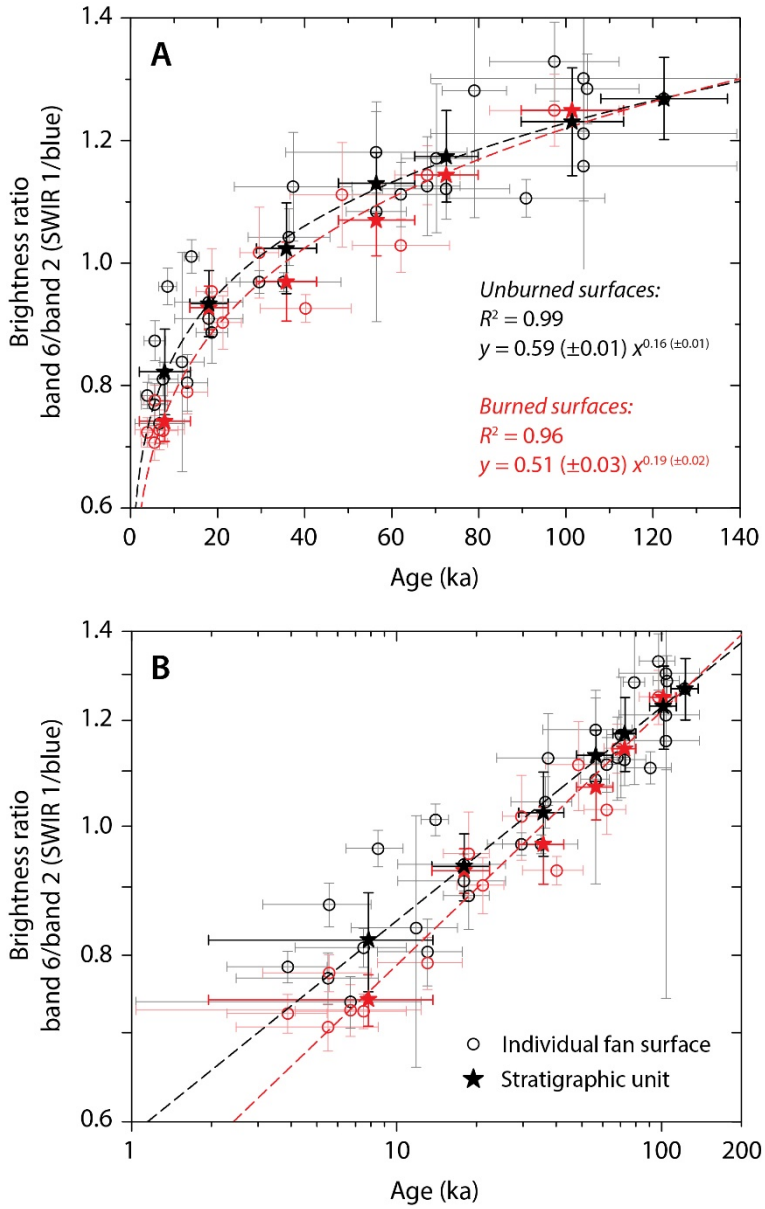

Fig. 5. (A) Brightness ratio of band 6 (SWIR 1)/band 2 (blue) for each alluvial fan surface (open circles) and averaged for each stratigraphic unit (stars). Burned and unburned sampling sites are shown in red and black, respectively. There is a gradual increase in the brightness ratio with age, in agreement with Fig. 4. The stratigraphic averages are fitted with a power law regression, which predicts a starting ratio of 0.5-0.6 (when age = 0 ka), has an exponent of 0.16-0.19 and describes the data well (R^2 = 0.96-0.99). The regression parameters are identical within uncertainty if fitted to the individual fan surfaces, and R^2 decreases to 0.86 (non-burned surfaces) and 0.90 (burned surfaces). (B) The same data plotted in log-log form;

the brightness ratio is a good predictor of fan surface age with the greatest sensitivity between 10-100 ka.

4.2. Visible-IR reflectance of surface samples

We used an ASD TerraSpec4 spectro-radiometer to measure high-resolution reflectance spectra (1 nm sampling interval) for the 4 surface sediment samples shown in Fig. 2c. The results are shown in Fig. 6a as reflectance (normalised to a white spectralon plate) from 0.35 to 2.5 μm. The reflectance of all samples increases significantly from 0.5-1.0 μm, at a rate that increases with surface age. The Q4 and Q3 samples are comparable in terms of overall reflectance, however the Q2c sample is brighter and the Q2b sample is even brighter still, particularly at SWIR wavelengths (>1.4 μm). In agreement with Fig. 4, older samples reflect more strongly at longer wavelengths relative to VIS blue wavelengths (~0.475 μm); a pattern that is similar in all 4 samples. There are three notable absorption features centred at 1.4, 1.9 and 2.2 μm; these become slightly deeper and more pronounced with age, indicating a greater quantity of particular minerals. In the inset panel of Fig. 6a we plot the area of the 2.2 μm absorption feature against surface age for each sample; this peak is associated with illite abundance and increases with age. Automated analysis of these spectra based on published library mineral spectra indicate the presence of illite and muscovite in the three youngest samples, and additionally iron oxide and kaolinite in the oldest Q2b sample. In Fig. 6b we compare these results with spectra for selected reference minerals after Clark et al. (2007), and we revisit this in the Discussion.

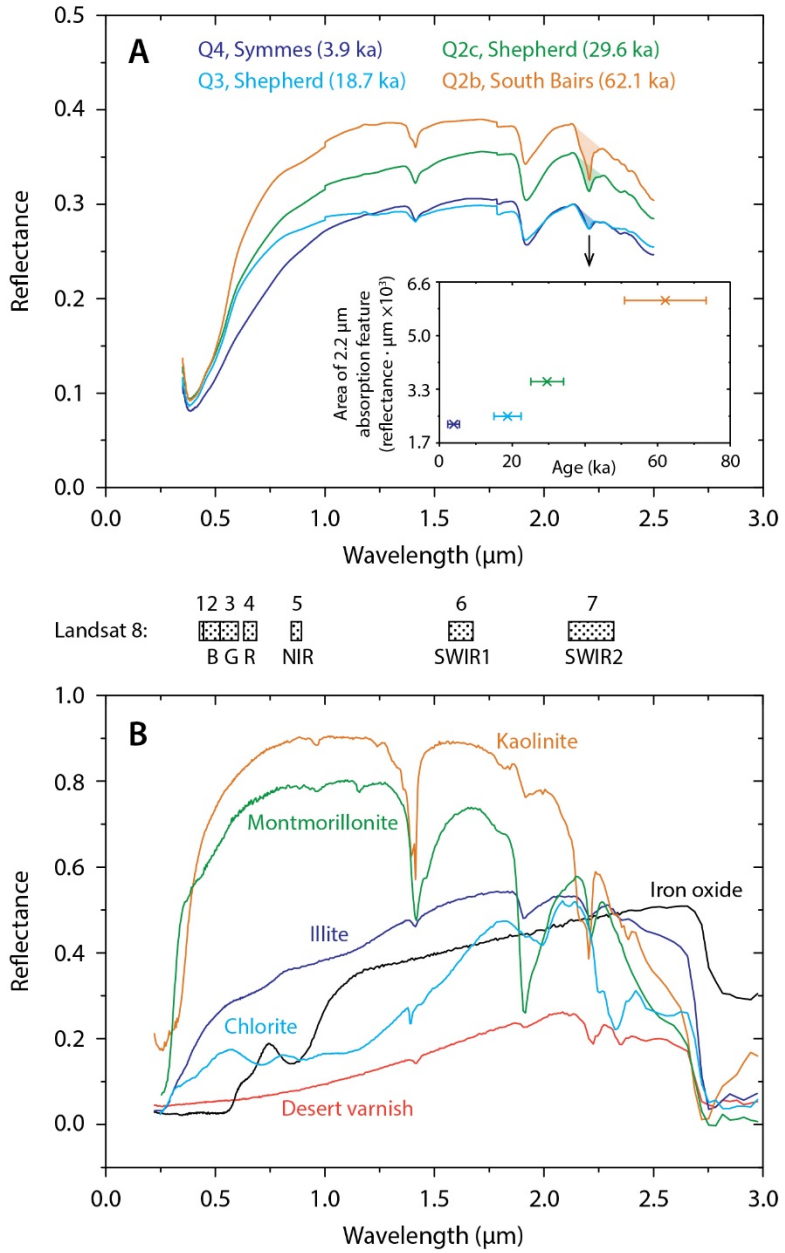

Fig. 6. Visible-infrared reflectance spectra for (A) 4 surface gravel samples from the Owens Valley fans. The inset panel shows the area of the (shaded) 2.2 µm absorption feature (associated with illite abundance) plotted against sample age. (B) reference minerals after Clark et al. (2007). The wavelength windows of Landsat 8 bands 1-7 are shown for comparison.

4.3. XRD analysis of clay fraction

To investigate any changes in the composition of the fan surface sediments over time, we performed XRD analyses of two samples with ages differing by ~60 kyr (Q4 ~4 ka and Q2b ~62 ka; see Methods). Bulk analyses on crushed gravels from both surface samples showed clear peaks associated with quartz, albite, microcline, hornblende and augite, i.e., characterising the granitic composition of the sediments, which were eroded from granite plutons in the southern Sierra Nevada (data not shown). Mineralogical changes associated with in-situ weathering on the fan surfaces are therefore likely to be subtle, so we also separated the clay fraction, in which most alteration minerals form, and performed XRD analyses on these (Fig. 7). The younger Q4 sample is from a ~4 ka surface, and has three pronounced peaks associated with illite, a moderate peak associated with microcline (reflecting the bulk composition), and two very small peaks associated with chlorite. Results were similar for the older Q2b sample (~62 ka), but the main illite peak at 8° is more pronounced, and a secondary peak associated with kaolinite is present at ~12°; this is absent from the Q4 sample. These results agree with the automated analysis of the visible-IR spectra in Fig. 6a, which identified the presence of illite in all samples, and minor kaolinite in only the oldest Q2b sample.

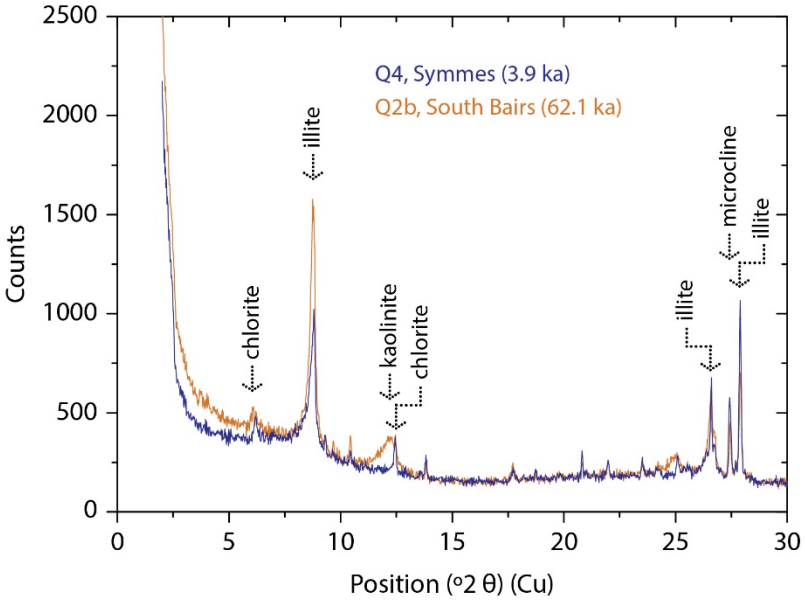

Fig. 7. Clay fraction XRD results for the Q4 and Q2b surface samples. Only low angles are displayed to focus on clay absorption features. The main peaks are associated with illite and microcline. A broad kaolinite peak appears in the Q2b sample at ~12 °, which is absent from the Q4 sample. There are also small peaks associated with chlorite. No peaks were observed associated with any other clay minerals.

5. Discussion

These studied alluvial fan surfaces in Owens Valley, California, exhibit visible-infrared reflectance patterns that evolve over time. Younger surfaces reflect more brightly at visible wavelengths (e.g., red, green and particularly blue light), and as the surfaces age they become progressively brighter in the near- to short-wave infrared wavelengths (Fig. 3). Normalised relative brightness, as recorded in Landsat 8 bands 1-7, show a clear sensitivity to fan surface age (Fig. 4) and this can be transformed into a brightness ratio that increases non-linearly over time (Fig. 5). A band ratio is the simplest strategy for exploiting the age-brightness relationship for these particular alluvial fans, and is sensitive to surface age for at least 120 ka. All of the 33 dated fan surfaces we sampled show equivalent patterns in wavelength-dependent brightness, meaning the trend is consistent for all surfaces. These results confirm that useful information about alluvial fan surface age is recorded by multispectral satellite imagery.

5.1. Origin of the age-reflectance relationship

What does this signal physically represent? It shows that there are age-dependent compositional differences between the fan surfaces, and given the uniformly granitic lithology in the Sierra Nevada parent catchments we make the robust assumption that there has been no time-dependent change in the original composition of sediments delivered to the fans. In other words, we attribute the signal to in-situ ageing of the fan surfaces.

Results from VNIR-SWIR spectro-radiometry (Fig. 6a) and XRD analysis (Fig. 7) show the composition of the surface sediment samples subtly changes with age. Specifically, illite is being produced as a secondary clay mineral. We attribute this to the weathering of feldspars, which commonly produces illite when granitic rocks are weathered in arid to semi-arid environments (Reheis, 1990; Velde & Meunier, 2008). As shown by Fig. 6b, the production of illite acts to increase reflectance in the SWIR wavelengths (i.e., bands 6 and 7) relative to the visible wavelengths (bands 1-4), and can therefore explain the results in Figs 3-5. Illite also exhibits VNIR-SWIR absorption features that closely match those identified in the sediment samples from the fans (Fig. 6a), suggesting it is an important component of the fan surface material. We also observe an increase in the area of the 2.2 μm absorption feature as a function of surface age (inset panel, Fig. 6a), which indicates illite production over time. Kaolinite can also be produced by the weathering of granites, albeit more commonly in wetter environments (White et al., 2001; Velde & Meunier, 2008). We identify very minor secondary production of kaolinite after ~60 ka, but this is much less significant than illite production (Fig. 7) and cannot explain the spectro-radiometry measurements in Fig. 6. This implies that illite is the dominant clay weathering product influencing spectral brightness, and kaolinite production is not a significant driver of the age signal we document in Landsat-8 imagery. We also note very minor XRD peaks associated with chlorite (Fig. 7). Chlorite is a common weathering product in arid soils (Goudie, 2013), although it does not appear to be a major component of our field specimens nor does it match the sediment sample spectra in Fig. 6a. However, if a small amount of chlorite is being produced by weathering then it would also act to increase the SWIR rather than visible brightness, like illite (Fig.6b), and could therefore make a small contribution to the observed age-brightness relationship.

Other weathering processes clearly occur in addition to clay production. For example, iron is typically an immobile element during weathering and secondary iron oxides form as coatings on the surfaces of particles during the weathering of granites (Middelburg et al., 1988). On dryland alluvial fan surfaces in Crete this has been shown to be a gradual process lasting

several 10s of kyr (Ferrier & Pope, 2012). Augite and hornblende—both iron-bearing silicates that we identify in the bulk composition of the granites in our study area (see section 4.3)—release iron during weathering, which precipitates as iron oxides on particle surfaces (White & Yee, 1985). Automated analysis of the spectro-radiometry data in Fig. 6a detects the presence of iron oxide in the older Q2b sample, and the gradual increase in iron oxide is clearly discernable in the rust-red discolouration of older fan surfaces in the field, as well as in gravel specimens (Fig. 2). As shown by the reference spectra in Fig. 6, the in-situ production of iron oxide would also act to increase reflectance in NIR and SWIR wavelengths relative to visible wavelengths, in a similar way to illite. Therefore, we interpret that the formation of secondary illite and iron oxide are both occurring on these fan surfaces, and simultaneously contribute to the age-brightness relationship we detect in Landsat 8 imagery.

In addition to forming in-situ, iron oxides—and other metal oxides, e.g., manganese oxides—can be supplied by airborne dust (Bowman, 1982). In arid environments, allogenic metal oxides typically accrete on particle surfaces, along with clays such as illite, to produce a dark brown-black outer veneer described as desert varnish (Bull, 1991; DiGregorio, 2005; Goudie, 2013). Trace amounts of desert varnish can be observed on some boulders on the oldest fan surfaces in Owens Valley, dating to ~100 ka (see Fig. 2b). Given that illite and iron oxide are two of the primary constituents of desert varnish, it displays a similar spectral profile to these minerals (Fig. 6b) and could also contribute to the changes in fan surface reflectance over time. However, we observed only minimal degrees of clast varnishing in Owens Valley (Fig. 2b), and do not detect a substantial overall decrease in surface albedo with age (Fig. 3), which typically occurs on fan surfaces where desert varnish formation is more pronounced (Stock et al., 2007). Therefore, the accretion of varnish may contribute to the age-brightness relationships shown in Figs 3-5, but it most likely plays a smaller role than the in-situ production of clays and iron oxide by weathering.

We rule out the accumulation of soil carbonate and salts on the fan surfaces over time; while this has been documented in some dryland settings (Blisniuk et al., 2012; Oerter et al., 2016),

we did not observe any evidence for carbonate or salt accumulation in the field. We also exclude textural changes on the fan surfaces (e.g., the diffusional loss of relief, desert pavement formation, changes in particle size distributions, or the shattering and physical breakdown of clasts), because these may change the overall brightness of a surface (Shipman & Adams, 1987), but cannot explain a change in composition or in the shape of the spectral profile. We also find that burned and unburned surfaces demonstrate very similar spectral evolution as a function of surface age, albeit burned patches of the fans are brighter overall and exhibit marginally lower band 6/band 2 ratios than unburned surfaces (Fig. 5). This suggests that surface vegetation cover plays a role in determining the total brightness of these fan surfaces (cf. Ustin et al., 1986; Smith et al. 1990a,b), but that it is not significantly related to their long-term (~100 ka) evolution. This finding is in agreement with previous work by Ustin et al. (1986) that derives the perpendicular vegetation index (PVI) for these fan surfaces in Owens Valley; this index does not discriminate any of the stratigraphic units mapped by D'Arcy et al. (2015, 2017b).

In summary, sustained illite production from the weathering of feldspars can explain the observed increase in relative SWIR brightness over time (e.g., Fig. 5) and is compatible with our XRD and spectro-radiometry results, and the weathering environment in Owens Valley. Kaolinite may also be produced in small amounts over time, but this would act to decrease the band 6/band 2 ratio (see Figs 5 and 6) and therefore does not likely play a significant role in the spectral evolution we document in Figs 3-5. In-situ iron oxide formation is another reasonable explanation for the age-reflectance trend, and is compatible with our field observations for surfaces that span several 10s of kyr (Fig. 2). A minor contribution to the spectral evolution could also be made by the accretion of desert varnish, although our field observations and the minor decrease in surface albedo with age both suggest this plays a smaller role. Therefore, we interpret the gradual increase in SWIR brightness (relative to visible, e.g. band 2) to be a composite signal that integrates multiple weathering and alteration processes, but is primarily driven by the in-situ production of secondary illite and iron oxide.

5.2. Surface weathering constraints from field data

In the southwest United States, reported indices of soil development and pedogenic clay content produce a linear trend on log-log plots against surface age, mirroring our results in Fig. 5b. This includes data from the Whipple Mountains (Bull, 1991) and the San Joaquin Valley (Harden, 1987) in California, as well as Owens Valley specifically (Zehfuss et al., 2001). Field measurements of the soil profile development index for the Birch creek fan—one of our target fans, see Fig. 1—increase sub-linearly with age following a power law with an exponent of about 0.3 (Zehfuss et al., 2001), compared to an exponent of ~0.2 for the band 6/band 2 brightness ratio shown in Fig. 5. We refer the reader to Zehfuss et al. (2001) for a detailed description of soil development on these fan surfaces. As these data come from our exact study area, a match between the rate of pedogenesis over ~100 kyr and the rate of change of the band 6/band 2 ratio (which we attribute to the production of secondary illite and iron oxide) supports our interpretations.

Debris flow fan surfaces in the Sfakia region of Crete, Greece, have been dated and described by Ferrier & Pope (2012) and are comparable to the Owens Valley fans in terms of their sedimentology and climatic setting. Ferrier & Pope (2012) identified the in-situ formation of pedogenic iron oxides and clays in dated fan surfaces, and demonstrated that their gradual accumulation can be used to distinguish abandoned depositional units. Furthermore, the authors used field-based reflectance spectroscopy to show that these compositional changes are recorded by the multispectral reflectance from the sediments. These data are in agreement with our interpretations for the Owens Valley fans, and similarly show that the increase in secondary clays and oxides is non-linear and persists over a ~100 kyr timescale. This study area has a comparable semi-arid climate and average annual temperature (~18 °C) to Owens Valley, although the source lithologies are variable and include marbles, siliciclastic sediments, schists and quartzites (Ferrier & Pope, 2012). The Sfakia alluvial fans provide

evidence that age-reflectance relationships, similar to the one we describe for Owens Valley, exist for other dryland alluvial fan systems as well.

Although we interpret that the accretion of desert varnish plays a small role in the relative increase in SWIR brightness with fan age in Owens Valley (see section 5.1), varnishing has also been shown to darken desert pavements in the Whipple Mountains, California, following a sub-linear power law over 10s-100s of kyr (Bull, 1991). In this area, approximately half of the surface darkening associated with the formation of desert varnish occurs in the first ~50 kyr of varnishing, and around two-thirds by ~100 kyr (Bull, 1991). This rate of alteration is comparable with the rate and shape of change in the band 6/band 2 brightness ratio we show in Fig. 5.

5.3. Applications for mapping and correlating alluvial fan surfaces

The ability to discriminate alluvial fan surfaces by age using multispectral imagery has obvious applications for mapping Quaternary deposits, even without age control. Imagery such as Landsat-8 can be used for preliminary mapping of alluvial fan systems before going to the field, and for site selection when sampling for absolute dating.

Figure 8 illustrates these opportunities with an oblique view of the George Creek and South Bairs Creek fans. Standard aerial imagery (Fig. 8a) does allow some mapping, e.g., the raised terrace to the south of the George Creek fan and the raised lobe within the South Bairs Creek fan are both clearly older than surrounding surfaces and more orange in colour, while more recent deposits have a rougher texture. However, when a Landsat bands 642 (RGB) colour composite is overlain (Fig. 8b), the differences between individual fan surfaces become much more pronounced. The boundaries between fan surfaces, as mapped in the field by D'Arcy et al. (2015), are highlighted with white lines. Isolated islands of older fan material can now be identified accurately, and the boundaries of fan lobes become clear. Some fan surfaces can only be identified using the false colour composite, e.g., the various 'islands' of older fan

material, which appear yellow, grey and brown-red in colour. Field mapping and absolute surface dating has confirmed these patches of material each have distinct ages (D'Arcy et al., 2015). Areas of older exposed fan material can otherwise be quite small and difficult to identify in aerial imagery, but it is important to locate them because they offer valuable snapshots of sedimentation at a certain point in time.

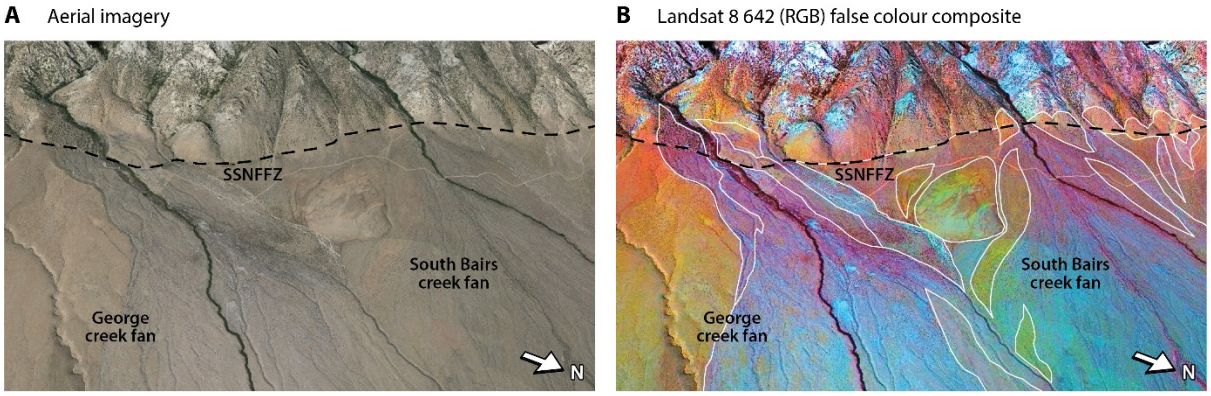

Fig. 8. Oblique view of the George Creek and South Bairs Creek fans taken from Google Earth, showing (A) aerial imagery and (B) a Landsat 8 642 (RGB) false colour composite with distinct fan surfaces outlined in white. *SSNFFZ* = Southern Sierra Nevada Frontal Fault Zone. For scale, the distance between the two major streams where they cross the SSNFFZ is ~3 km.

As well as mapping fan boundaries, multispectral imagery can be used to correlate surfaces with similar ages due to the consistent age-reflectance relationship (Fig. 5). For example, the most recent Holocene (Q4) deposits in Fig. 8b have equivalent ages (D'Arcy et al., 2015) and identical blue-purple appearances in the false colour composite. The orange Q1 terrace on the George Creek fan (on the far left of Fig. 8b) can also be correlated upstream towards the catchment across the zone now incised by the modern channel. This provides useful

morphological information, i.e., that the George creek fan was significantly backfilling at the time of Q1 deposition, but has since prograded and entrenched at the apex.

The relationship between Landsat-8 spectral properties and fan surface age offers new opportunities for (i) preliminary mapping of alluvial fan surfaces prior to field work, or validation of maps after field work; (ii) placing surfaces in a relative chronological order; (iii) correlating fan surfaces of similar age and interpreting their morphological and cross-cutting relationships; and (iv) choosing sampling sites for absolute dating efforts.

5.4. Applications for estimating fan surface ages

Additionally, our results also raise the prospect of predicting absolute alluvial fan surface ages using remotely-sensed imagery, in areas where a suitable age-reflectance calibration can be established. We first explore the potential for this in Fig. 9 by performing a retrospective test, using the Owens Valley calibration data from this study. Subsequently, we apply this technique to neighbouring fans in Death Valley to compare and evaluate this approach in a different location.

For each sampled fan surface (and the stratigraphic averages) in our Owens Valley data set, we have taken the measured band 6/band 2 brightness ratio and calculated the age that would be predicted using the regression in Fig. 5 for unburned surfaces. We perform this test for unburned surfaces with normal semi-arid vegetation cover as this scenario is most commonly encountered, although the similarity of the regressions in Fig. 5 show that there is no significant difference in the scatter or rate of change of surface brightness on burned surfaces. In Fig. 9a, these predicted ages are plotted against the actual fan surface ages described by D'Arcy et al. (2015; 2017b). If a point falls on the 1:1 line there is a perfect match between the predicted and actual ages, and the further a point falls from the 1:1 line the poorer the predicted age. In Fig. 9b we show the differences between the predicted and actual surface ages, plotted

against the actual age, and the inset panel (c) shows normalised frequency distributions of these discrepancies.

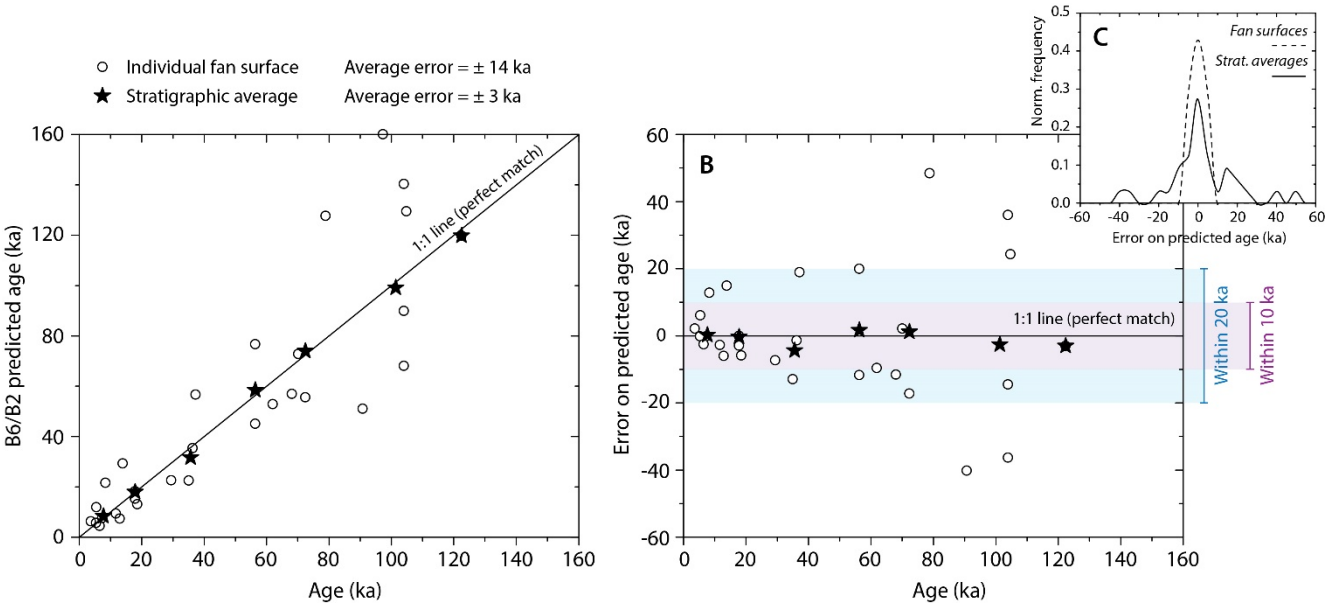

Fig. 9. (A) Comparison of predicted fan surface ages using the relationship in Fig. 5 for unburned surfaces, with the actual fan surface ages. (B) Plot of the error between the predicted and actual fan surface ages, compared with actual fan surface age. (C) Normalised frequency distributions of the error on fan surface age (predicted using the relationship in Fig. 5) compared with the actual fan surface ages.

The positive correlation between predicted and actual ages demonstrates that it is possible to predict the absolute age of an alluvial fan surface using Landsat 8 imagery, in locations such as Owens Valley, where lithology and environmental boundary conditions are uniform across space and an accurate age calibration can be established. For individual surfaces there is considerable scatter, and figures 9b and 9c show that most estimated ages are correct within 10-20 ka, but in some cases older than ~80 ka this error might be >40 ka. These uncertainties are substantially larger than the uncertainties on ages derived from techniques like cosmogenic radionuclide exposure dating, OSL, or radiocarbon dating. Nonetheless, they are

age estimates that can be derived quickly and easily from freely-available Landsat-8 imagery, offer a useful starting point before field sampling, and have a temporal range of at least 100 ka. This dating timescale is relevant for studies looking at the effects of both climate and tectonics on alluvial fans, and is agreement with other studies that show relationships between the ages of alluvial surfaces in drylands and their colour (Dickerson et al., 2015) and roughness (Hetz et al., 2016).

The results for the stratigraphic averages in Fig. 9 (black stars) show that binning multiple surfaces of equivalent age leads to a very significant improvement in this method for predicting surface age. Most of these predicted ages lie within ~5 ka across the full timespan studied, and this level of uncertainty is comparable to conventional dating techniques. This is important because it means that fan surfaces ages predicted using multispectral imagery are likely to be more accurate if surfaces are already mapped and organised into a simple relative stratigraphy. Section 5.3 and Fig. 8 show that this relative organisation can be done simply and without prior age control, and traditional field-based techniques for surface mapping (see section 1) can also be used to develop a relative stratigraphy.

We emphasise that calibration with known fan surface ages is needed before multispectral imagery can be used to make robust age estimates for fan surfaces in a given study area (i.e., a location-specific version of Fig. 5). We also point out that substantially greater vegetation cover might obscure any reflectance signals related to the weathering and evolution of fan surfaces and alluvial sediment, so similar results are only likely to be found in arid or semi-arid landscapes where vegetation cover is sparse. However, these are also landscapes where there is little/no opportunity for radiocarbon dating, making alternative dating methods particularly useful. The analyses in Figs 5 and 9 make use of the particularly high spatial and temporal density of surface age constraints available for the Owens Valley fans, to reveal that it is possible to estimate the absolute ages of these fan deposits remotely. This finding has applications for local geomorphological and sedimentological studies that require data about

the ages of fan surfaces, e.g., to determine whether sedimentary deposits in basins record signals of past climate changes or tectonics (D'Arcy et al., 2017b).

5.5. Comparison with Death Valley

Our study has focused on the Owens Valley fans because they have been dated at a very high resolution in both time and space (see section 2), and therefore allow us to constrain the spectral evolution of surfaces in great detail (Fig. 5). Nonetheless, age constraints have been reported for alluvial surfaces in comparable environments. We therefore explore whether other alluvial fan systems show comparable spectral signatures over time. In Fig. 10, we perform a comparison between our results from Owens Valley, and four surfaces on the Backthrust Canyon and Moonlight Canyon alluvial fans in neighbouring Death Valley, California. We have selected these fans for comparative study as they sit at precisely the same latitude as the Owens Valley fans, 85 km to the east, and both have modern surfaces (0 ka) and abandoned surfaces dated with ^{10}Be cosmogenic nuclides to 70 ka (+22/-20 ka) by Frankel et al. (2007b). These appear blue and red, respectively, in a Landsat-8 bands 642 (RGB) false colour composite (Fig. 10a) and thus also exhibit a spectral maturation with age.

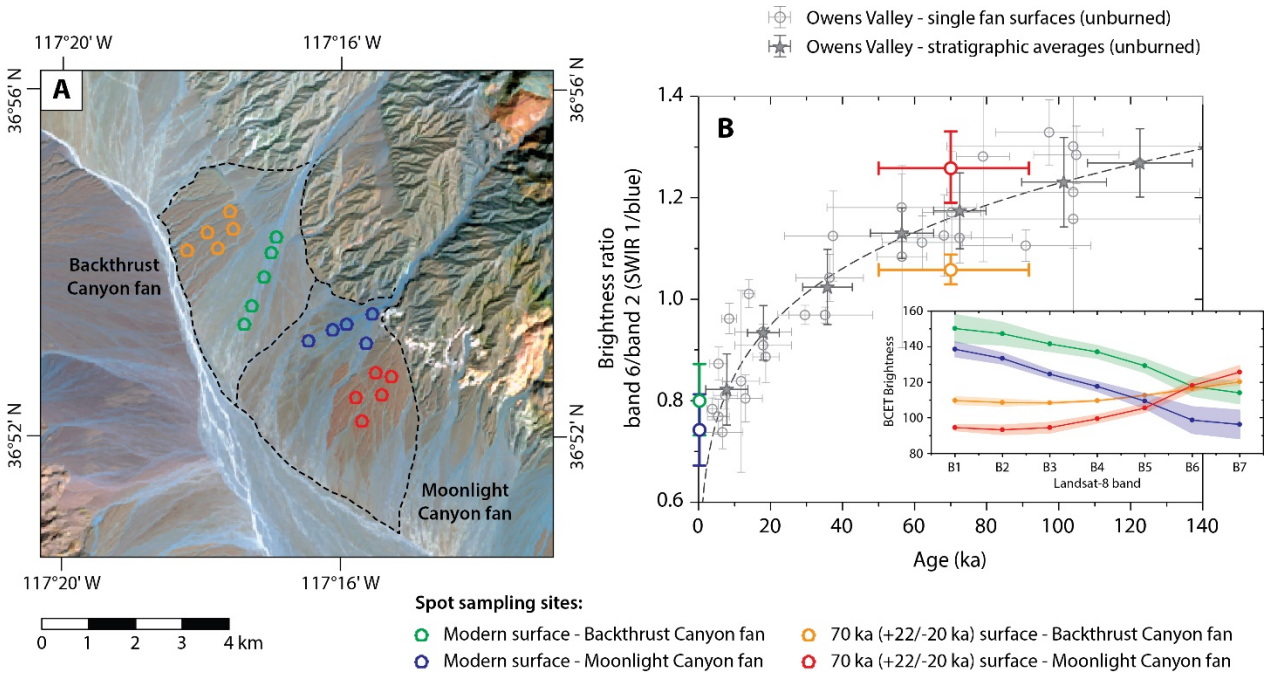

Fig. 10. (A) Landsat-8 false colour composite (642 RGB, date: 14th February 2013) locating the Backthrust Canyon and Moonlight Canyon alluvial fans in Death Valley, California. BCET brightness was obtained for each Landsat-8 band for the modern fan surfaces (green and blue spots), and abandoned fan surfaces (yellow and red spots) dated to 70 ka (+22/-20 ka) by Frankel et al. (2007b) using ^{10}Be cosmogenic nuclides. (B) The band 6/band 2 ratio is calculated for each fan surface, and plotted alongside the data for unburned surfaces in Owens Valley (grey symbols and regression, see Fig. 5). The inset panel shows the BCET brightness spectra across bands for each surface.

Death Valley is another arid basin adjacent to Owens Valley. The average climate is slightly warmer and drier than Owens Valley (average temperature 25 °C, average annual precipitation ~60 mm; Western Regional Climate Center, 2015) and vegetation cover is sparser (<10% coverage of arid shrub communities), but both are dryland basins filled by extensive alluvial fan complexes, situated in the rain shadow of the Sierra Nevada and with

similar climatic histories during the past ~100 kyr (Phillips, 2008; also see D'Arcy et al., 2017a for a review of these fans and their geomorphic context).

We followed the same analytical procedure applied to the Owens Valley surfaces (see Methods). First, we downloaded a cloud-free Landsat-8 scene (path 40, row 35, 14th, imaged on February 2013) and applied the BCET technique to the scene area shown in Fig. 10a, before spot-sampling brightness in each band for the two modern and two ~70 ka surfaces (using five 200 m-diameter spots placed on stable and representative parts of each fan surface). Data are provided in the supplementary information. Brightness spectra in Fig. 10b (inset) show similar patterns with age to the Owens Valley fans (Figs 3 and 4), with younger surfaces reflecting more brightly in the visible bands and older surfaces reflecting more brightly in the SWIR bands. A band 6/band 2 ratio is plotted against surface age in Fig. 10b (coloured symbols), and for comparison we show the data and regression for the unburned Owens Valley fan surfaces in grey (from Fig. 5).

The Death Valley fans only have modern surfaces and ~70 ka surfaces (with slightly larger age uncertainties compared to the deposits in Owens Valley), so it is not possible to derive the overall shape of the brightness-age relationship. Their surfaces also comprise mixed volcanic and carbonate sediments (Niemi, 2012) meaning weathering pathways could differ from the Owens Valley fans, although the presence of feldspar-bearing volcanics does allow the production of secondary illite and iron oxides. Nonetheless, the band 6/band 2 ratio increases with surface age from 0.7-0.8 (modern) to ~1.05-1.25 by ~70 ka. The direction and timescale of this change in the band 6/band 2 ratio is comparable to our observations from Owens Valley, indicating that such a band ratio can increase with fan surface age over 10s of ka in other dry landscapes. This raises the possibility of our approach being used to quantify age-brightness relationships for alluvial fan surfaces elsewhere. However, the two ~70 ka surfaces do not fall on the band ratio vs age regression obtained for the Owens Valley surfaces (Fig. 10b). The dating uncertainty is larger for these surfaces (i.e., they could range between ~50 ka and ~90 ka), but this observation additionally suggests that the differences in lithology,

weathering pathways, and climate between the Owens Valley and Death Valley sites have a significant effect on the band 6/band 2 ratio. These environmental variables, among others, could change the magnitude of spectral changes with time, or the rate of spectral change (or both). As a result, the rates and patterns of spectral change with surface age are likely to vary between basins, and scene-specific age-brightness calibrations must be derived for individual study areas using existing age control before they can be used to make additional age correlations at that location. Of course, the age-brightness calibration we report for Owens Valley is not directly transferable to fan surfaces with different compositions or situated in different climates. However, it also means that the parameters of the age-brightness regression could sensitively record information about weathering rates on alluvial surfaces, and could potentially be used as a novel tool to investigate weathering kinetics.

5.6. Opportunities for future work

Future studies could derive age-brightness calibrations for alluvial fan surfaces in (i) similar environments to Owens Valley, to test our findings; and (ii) study areas with various climates, rock types and weathering conditions, to determine the sensitivity of the age calibration to these factors. We anticipate that the age model will vary to different extents between study areas. It is likely to depend on climatic factors that govern weathering rates like temperature and moisture availability (Dixon et al., 2016), the initial composition of the fan material (the Owens Valley fans have a granitic mono-lithology, and systems with a mixture of rock types may have more complicated weathering systems), the various weathering processes occurring on the surfaces and their rates, the intensity of processes like desert varnish accretion, and any allogenic materials like dust, salts or soil carbonate that are delivered to surfaces over time. While our comparison with neighbouring Death Valley (section 5.5) suggests that our analytical approach could be applied to alluvial surfaces in other dryland environments, systematic analyses are now warranted in multiple study areas with detailed age control to explore this in detail.

Our results could also be compared with multispectral imagery from different satellites, for example ASTER or Sentinel-2, which has a higher spatial resolution. Hyperspectral imagery, e.g., Hyperion, could provide additional information about the weathering processes that occur on alluvial fans, and their rates and mineralogical products. Other types of remotely-sensed data could also be explored, e.g., Hetz et al. (2016) show that radar backscatter can be used as a predictor of alluvial fan surface age in Israel and Jordan, and combining multispectral imagery with other types of data might strengthen regional age calibrations (cf., Farr and Chadwick, 1996). Finally, while we find that illite and iron oxides are the dominant weathering products driving the age-reflectance relationship in Owens Valley, it is likely that a range of more subtle and complex weathering pathways take place on these fans as well. More comprehensive studies of weathering reactions and secondary mineral formation on dryland alluvial fan surfaces could constrain these pathways in more detail. Furthermore, the parameters of the brightness-age regression are likely to contain information about the long-term (10^3 to 10^5 year) kinetics of weathering of alluvial surfaces, and may present an opportunity to quantify the sensitivity of these kinetics to environmental parameters.

6. Conclusions

Alluvial fan surfaces composed of granite-sourced sediment and with ages spanning >100 kyr in Owens Valley, California, exhibit systematic changes in their VNIR and SWIR brightness over time. These surfaces gradually become brighter in the short-wavelength infrared relative to visible wavelengths, and this is captured by Landsat 8 imagery. We spot-sample 33 distinct, dated fan surfaces to constrain the rate and pattern of this spectral evolution. A simple brightness ratio between Landsat-8 bands 6 and 2 increases predictably with fan surface age following a power law relationship that is compatible with independent observations of post-depositional weathering processes on dryland alluvial fans. The spectral evolution of these fan surfaces as a function of their age is relatively insensitive to vegetation cover, as

demonstrated by a comparison of wildfire scars and unburned areas of the alluvial fans. We use VNIR and SWIR spectro-radiometry and XRD analysis of surface sediment samples to interpret that the age-brightness relationship is primarily driven by the in-situ production of secondary illite and iron oxide, although it is a composite signal that could also include smaller contributions from other weathering products (e.g., chlorite) and the accretion of desert varnish. The ability to discriminate alluvial fan surfaces by age using multispectral imagery has useful applications for the mapping of alluvial fans and site selection for absolute dating. The high density of surface age control in our study area means our findings also present a new opportunity for predicting the absolute ages of alluvial fan deposits remotely. By performing a retrospective test using our calibration data from Owens Valley, we show that multispectral imagery can provide useful age estimates over 10-100 ka timescales where a robust age calibration is available. We also document an age-brightness relationship for comparable fan surfaces in neighbouring Death Valley, California. Therefore, we anticipate that in other dryland basins with existing independent age control, multispectral imagery could present a valuable opportunity for extending surface age models to un-dated surfaces, as well as investigating the long-term weathering dynamics of sedimentary surfaces.

7. Acknowledgements

This project was kindly supported by postgraduate research grants awarded to MD by the British Society for Geomorphology, the Geological Society of London, the International Association of Geomorphologists and the Jeremy Willson Charitable Trust. ACW was supported by the Royal Society. The assistance of ASD Inc. (PANalytical) in checking the identification of our mineral spectra is gratefully acknowledged. We thank the associate editor Tim McVicar, and three anonymous reviewers and Joel Roskin for their helpful comments.

8. References

Al Farraj, A. & Harvey, A.M. (2000) Desert pavement characteristics on wadi terrace and alluvial fan surfaces: Wadi Al-Bih, U.A.E. and Oman. *Geomorphology,* **35**, 279-297.

Armitage, J.J., Duller, R.A., Whittaker, A.C. & Allen, P.A. (2011) Transformation of tectonic and climatic signals from source to sedimentary archive. *Nature Geoscience,* **4**, 231-235.

Bateman, P.C. (1992) Plutonism in the central part of the Sierra Nevada batholith, California. *United States Geological Survey Professional Paper* 1483, pp. 186.

Benson L.V., Burdett J.W., Kashgarian M., Lund S.P., Phillips F.M., & Rye R.O. (1996) Climatic and hydrologic oscillations in the Owens Lake basin and adjacent Sierra Nevada, California. *Science,* **274**, 746-749.

Beratan, K.K. & Anderson, R. (1998) The use of Landsat Thematic Mapper data for mapping and correlation of Quaternary geomorphic surfaces in the southern Whipple Mountains, California. *International Journal of Remote Sensing*, **19**, 2345-2359.

Blisniuk, K., Oskin, M., Fletcher, K., Rockwell, T. & Sharp, W. (2012) Assessing the reliability of U-series and 10Be dating techniques on alluvial fans in the Anza Borrego Desert, California. *Quaternary Geochronology*, **13**, 26-41.

Bierman, P. & Gillespie, A. (1991) Range fires: A significant factor in exposure-age determination and geomorphic surface evolution. *Geology*, **19**, 641-644.

Bowman, D. (1982) Iron coating in recent terrace sequences under extremely arid conditions. *Catena*, **9**, 353-359.

Bull, W.B. (1991) *Geomorphic responses to climate change*. Oxford University Press, New York, USA, pp. 326.

Clark, R.N., Swayze, G.A., Wise, R., Livo, K.E., Hoefen, T.M., Kokaly, R.F. & Sutley, S.J. (2007) USGS Digital Spectral Library splib06a, *U.S. Geological Survey, Data Series 231*. Available online at: http://speclab.cr.usgs.gov/spectral.lib06/ds231/datatable.html

Crouvi, O., Ben-Dor, E., Beyth, M., Avigad, D. & Amit, R. (2006) Quantitative mapping of arid alluvial fan surfaces using field spectrometer and hyperspectral remote sensing. *Remote Sensing of Environment*, **104**, 103-117.

D'Arcy, M., Roda Boluda, D.C., Whittaker, A.C. & Carpineti, A. (2015) Dating alluvial fan surfaces in Owens Valley, California, using weathering fractures in boulders. *Earth Surface Processes and Landforms,* **40**, 487-501.

D'Arcy, M., Roda-Boluda, D.C. & Whittaker, A.C. (2017a) Measuring alluvial fan sensitivity to past climate changes using a self-similarity approach to grain-size fining, Death Valley, California. *Sedimentology*, 64, 388-424.

D'Arcy, M., Roda-Boluda, D.C. & Whittaker, A.C. (2017b) Glacial-interglacial climate changes recorded by debris flow fan deposits, Owens Valley, California. *Quaternary Science Reviews*, 169, 288-311.

Dickerson, R.P., Bierman, P.R. & Cocks, G. (2015) Alluvial fan surfaces and an age-related stability for cultural resource preservation: Nevada Test and Training Range, Nellis Air Force Base, Nevada, USA. *Journal of Archaeological Science: Reports*, **2**, 551-568.

DiGregorio, B.E. (2005) Rock varnish and the manganese oxide connection. *Analytical Chemistry*, **77**, 433-438.

Dixon, J.L., Chadwick, O.A. & Vitousek, P.M. (2016) Climate-driven thresholds for chemical weathering in postglacial soils of New Zealand. *Journal of Geophysical Research: Earth Surface*, **121**, 1619-1634.

Dühnforth M., Densmore A.L., Ivy-Ochs S., Allen P.A., Kubik P.W. (2007) Timing and patterns of debris flow deposition on Shepherd and Symmes creek fans, Owens Valley, California,

deduced from cosmogenic ^{10}Be. *Journal of Geophysical Research: Earth Surface* **112**, F03S15.

Farr, T.G. (1985) Age-dating volcanic and alluvial surfaces with multipolarization data. In: NASA/JPL Aircraft SAR Workshop Proceedings: JPL Publication 85-39, p. 31-36.

Farr, T.G. & Chadwick, O.A. (1996) Geomorphic processes and remote sensing signatures of alluvial fans in the Kun Lun Mountains, China. *Journal of Geophysical Research: Planets*, **101**, 23091-23100.

Ferrier, G. & Pope, R.J.J. (2012) Quantitative mapping of alluvial fan evolution using ground-based reflectance spectroscopy. *Geomorphology*, **175-176**, 14-24.

Frankel, K.L. & Dolan, J.F. (2007) Characterizing arid region alluvial fan surface roughness with airborne laser swath mapping digital topographic data. *Journal of Geophysical Research*, **112**, F02025.Frankel, K.L., Dolan, J.F., Finkel, R.C., Owen, L.A. & Hoeft, J.S. (2007a) Spatial variations in slip rate along the Death Valley-Fish Lake Valley fault system determined from LiDAR topographic data and cosmogenic ^{10}Be geochronology. *Geophysical Research Letters*, **34**, L18303.

Frankel, K.L., Brantley, K.S., Dolan, J.F., Finkel, R.C., Klinger, R.E., Knott, J.R., Machette, M.N., Owen, L.A., Phillips, F.M., Slate, J.L. & Wernicke, B.P. (2007b) Cosmogenic ^{10}Be and ^{36}Cl geochronology of offset alluvial fans along the northern Death Valley fault zone: Implications for transient strain in the eastern California shear zone. *Journal of Geophysical Research*, **112**, B06407.

Frankel, K.L., Dolan, J.F., Owen, L.A., Ganev, P. & Finkel, R.C. (2011) Spatial and temporal constancy of seismic strain release along an evolving segment of the Pacific–North America plate boundary. *Earth and Planetary Science Letters*, **304**, 565-576.

Gillespie, A.R. (1992) Spectral mixture analysis of multispectral thermal infrared images. *Remote Sensing of Environment*, **42**, 137-145.

Gillespie, A.R., Kahle, A.B. & Palluconi, F.D. (1984) Mapping alluvial fans in Death Valley, California, using multichannel thermal infrared images. *Geophysical Research Letters*, **11**, 1153-1156.

Goudie, A.S. (2013) *Arid and Semi-Arid Geomorphology*. Cambridge University Press, New York, USA, pp. 461.

Harden, J.W. (1987) Soils developed in granitic alluvium near Merced, California. In: Soil Chronosequences in the Western United States, *US Geological Survey Bulletin* **1590**, chapter A.

Hardgrove, C., Moersch, J. & Whisner, S. (2010) Thermal imaging of sedimentary features on alluvial fans. *Planetary and Space Science*, **58**, 482-508.

Harvey, A.M., Silva, P.G., Mather, A.E., Goy, J.L., Stokes, M. & Zazo, C. (1999) The impact of Quaternary sea-level and climatic change on coastal alluvial fans in the Cabo de Gata ranges, southeast Spain. *Geomorphology*, **28**, 1-22.

Hedrick, K., Owen, L.A., Rockwell, T.K., Meigs, A., Costa, C., Caffee, M.W., Masana, E. & Ahumada, E. (2013) Timing and nature of alluvial fan and strath terrace formation in the Eastern Precordillera of Argentina. *Quaternary Science Reviews*, **80**, 143-168.

Hetz, G., Mushkin, A., Blumberg, D.G., Baer, G. & Ginat, H. (2016) Estimating the age of desert alluvial surfaces with spaceborne radar data. *Remote Sensing of Environment*, **184**, 288-301.

Hibbitts, C.A. & Gillespie, A.R. (2008) Polarization of visible light by desert pavements. *Remote Sensing of Environment*, **112**, 1808-1819.

Hunt, C.B. & Mabey, D.R. (1966) Stratigraphy and structure, Death Valley, California. United States Geological Survey: Professional Paper 494-A, pp. 162.

Kahle, A.B., Shumate, M.S. & Nash, D.B. (1984) Active airborne infrared laser system for identification of surface rock and minerals. *Geophysical Research Letters*, **11**, 1149-1152.

Kahle, A.B. (1987) Surface emittance, temperature, and thermal inertia derived from Thermal Infrared Multispectral Scanner (TIMS) data for Death Valley, California. *Geophysics*, **52**, 858-874.

Kirby, E., Burbank, D.W., Reheis, M. & Phillips, F. (2006) Temporal variations in slip rate of the White Mountains Fault Zone, Eastern California. *Earth and Planetary Science Letters*, **248**, 168-185.

Le, K., Lee, J., Owen, L.A., Finkel, R. (2007) Late Quaternary slip rates along the Sierra Nevada frontal fault zone, California: Slip partitioning across the western margin of the Eastern California Shear Zone – Basin and Range Province. *Geological Society of America Bulletin*, **119**, 240-256.

Liu, J.G. (1991) Balance contrast enhancement technique and its application in image colour composition. *International Journal of Remote Sensing*, **12**, 2133-2151.

Liu, J.G. & Mason, P.J. (2016) Image Processing and GIS for Remote Sensing (2nd Ed.). John Wiley & Sons, Ltd., Oxford, United Kingdom, pp. 457.

Machette, M.N. (1985) Calcic soils of the southwestern United States. *Geological Society of America Special Paper*, **203**, 1-21.

Machette, M.N., Slate, J.L. & Phillips, F.M. (2008) Terrestrial cosmogenic-nuclide dating of alluvial fans in Death Valley, California. *U.S. Geological Survey Professional Paper 1755*, pp. 54.

Milana, J.P. (2000) Characterization of alluvial bajada facies distribution using TM imagery. *Sedimentology*, **47**, 741-760.

McFadden, L.D., Ritter, J.B. & Wells, S.G. (1989) Use of multiparameter relative-age methods for age estimation and correlation of alluvial fan surfaces on a desert piedmont, eastern Mojave Desert, California. *Quaternary Research*, **32**, 276-290.

National Oceanic and Atmospheric Administration (NOAA) National Climate Data Center (2014) http://www.ncdc.noaa.gov/ [accessed 2 January 2014].

Niemi, N.A. (2012) Geologic map of the central Grapevine Mountains, Inyo County, California, and Esmeralda and Nye Counties, Nevada. *Geological Society of America Digital Map and Chart Series*, **12**.

Noller, J.S., Sowers, J.M. & Lettis, W.R. (2001) Quaternary Geochronology: Methods and Applications. American Geophysical Union, pp. 582.

Oerter, E.J., Sharp, W.D., Oster, J.L., Ebeling, A., Valley, J.W., Kozdon, R., Orland, I.J., Hellstrom, J., Woodhead, J.D., Hergt, J.M., Chadwick, O.A. & Amundson, R. (2016) Pedothem carbonates reveal anomalous North American atmospheric circulation 70,000–55,000 years ago. *Proceedings of the National Academy of Sciences*, **113**, 919-924.

Owen, L.A., Frankel, K.L., Knott, J.R., Reynhout, S., Finkel, R.C. Dolan, J.F. & Lee, J. (2011) Beryllium-10 terrestrial cosmogenic nuclide surface exposure dating of Quaternary landforms in Death Valley. *Geomorphology*, **125**, 541-557.

Owen, L.A., Clemmens, S.J., Finkel, R.C. & Gray, H. (2014) Late Quaternary alluvial fans at the eastern end of the San Bernardino Mountains, Southern California. *Quaternary Science Reviews*, **87**, 114-134.

Phillips, F.M. (2008) Geological and hydrological history of the paleo-Owens River drainage since the late Miocene. In: Reheis, M.C., Hershler, R. & Miller, D.M (Eds) *Late Cenozoic drainage history of the southwestern Great Basin and lower Colorado River region: Geologic and biologic perspectives*. Geological Society of America Special Paper 439, Boulder, CO, USA, pp. 115-150.

Porat, N., Amit, R., Zilberman, E. & Enzel, Y. (1997) Luminescence dating of fault-related alluvial fan sediments in the southern Arava Valley, Israel. *Quaternary Science Reviews*, **16**, 397-402.

Regmi, N.R., McDonald, E.V. & Bacon, S.N. (2014) Mapping Quaternary alluvial fans in the southwestern United States based on multiparameter surface roughness of lidar topographic data. *Journal of Geophysical Research: Earth Surface*, **119**, 12-27.

Reheis, M.C. (1990) Influence of climate and eolian dust on the major-element chemistry and clay mineralogy of soils in the western Bighorn Basin, USA. *Catena*, **17**, 219-248.

Reheis, M.C., Slate, J.L., Sarna-Wojcicki, A.M. & Meyer, C.E. (1993) A late Pliocene to middle Pleistocene pluvial lake in Fish Lake Valley, Nevada and California. *Geological Society of America Bulletin*, **105**, 953-967.

Shipman, H. & Adams, J.B. (1987) Detectability of minerals on desert alluvial fans using reflectance spectra. *Journal of Geophysical Research*, **92** (B10), 10391-10402.

Smith, M.O., Ustin, S.L., Adams, J.B. & Gillespie, A.R. (1990a) Vegetation in deserts: I. A regional measure of abundance from multispectral images. *Remote Sensing of Environment*, **31**,1-36.

Smith, M.O., Ustin, S.L., Adams, J.B. & Gillespie, A.R. (1990b) Vegetation in deserts: II. Environmental influences on regional abundance. *Remote Sensing of Environment*, **31**, 27-52.

Sohn, M.F., Mahan, S.A., Knott, J.R. & Bowman, D.D. (2007) Luminescence ages for alluvial-fan deposits in Southern Death Valley: Implications for climate-driven sedimentation along a tectonically active mountain front. *Quaternary International*, **166**, 49-60.

Stock, J.D., Schmidt, K.M. & Miller, D.M. (2007) Controls on alluvial fan long profiles. *Geological Society of America Bulletin*, **120**, 619-640.

Ustin, S.L., Adams, J.B., Elvidge, C.D., Rejmanek, M., Rock, B.N., Smith, M.O., Thomas, R.W. & Woodward, R.A. (1986) Thematic mapper studies of semiarid shrub communities. *BioScience*, **36**, 446-452.

Velde, B. & Meunier, A. (2008) The origin of clay minerals in soils and weathered rocks. Springer-Verlag Berlin Heidelberg, pp. 406.

Wells, S.G., McFadden, L.D., Poths, J. & Olinger, C.T. (1995) Cosmogenic ^{3}He surface-exposure dating of stone pavements: Implications for landscape evolution in deserts. *Geology*, **23**, 613-616.

Western Regional Climate Center (2015) Climate summary for Death Valley, California (station 042319). Cooperative climatological data summaries. Western Regional Climate Center website, available at: http://www.wrcc.dri.edu/climatedata/climsum/ (accessed 10/10/2014).

White, A.F. & Yee, A. (1985) Aqueous oxidation-reduction kinetics associated with coupled electron-cation transfer from iron-containing silicates at 25°C. *Geochimica et Cosmochimica Acta*, **49**, 1263-1275.

White, A.F., Bullen, T.D., Schulz, M.S., Blum, A.E., Huntington, T.G. & Peters, N.E. (2001) Differential rates of feldspar weathering in granitic regoliths. *Geochimica et Cosmochimica Acta*, **65**, 847-869.

White, K., Drake, N., Millington, A. & Stokes, S. (1996) Constraining the timing of alluvial fan response to Late Quaternary climatic changes, southern Tunisia. *Geomorphology*, **17**, 295-304.

Woolfenden, W.B. (2003) A 180,000-year pollen record from Owens Lake, CA: Terrestrial vegetation change on orbital scales. *Quaternary Research*, **59**, 430-444.

Zehfuss, P.H., Bierman, P.R., Gillespie, A.R., Burke, R.M. & Caffee, M.W. (2001) Slip rates on the Fish Springs fault, Owens Valley, California, deduced from cosmogenic ^{10}Be and ^{26}Al and soil development on fan surfaces. *Geological Society of America Bulletin*, **113**, 241–255.

Yamamoto, M., Yamamuro, M. & Tanaka, Y. (2007) The California current system during the last 136,000 years: Response of the North Pacific High to precessional forcing. *Quaternary Science Reviews*, **26**, 405-414.

9. List of figure captions

Fig. 1. Maps locating the target fan surfaces in Owens Valley, California. (A) Landsat-8 false colour composite (642 RGB, date: 12th May 2013) showing spot sampling sites (unburned fan surfaces in black, burned surfaces in red). (B) Corresponding fan surface maps and ages are taken from D'Arcy et al. (2015). Younger surfaces appear more blue and older surfaces appear more orange.

Fig. 2. Field photographs of (A) a Q4 surface and (B) a Q1 surface taken in sunny conditions with constant camera settings and no contrast enhancement. These photographs show mature vegetation on these fans (unburned surfaces), which is dominated by sparse coverage of semi-arid shrubs (Ustin, 1986; Smith et al. 1990a). Sediment colour turns from grey to yellow with age and boulders become slightly varnished. (C) The change in colour can also be seen in gravel samples taken from various surfaces and photographed under constant lighting conditions. Ages are taken from D'Arcy et al. (2015).

Fig. 3. Average BCET spectral profiles (Landsat 8 bands 1-7) for each stratigraphic fan unit, showing the relative brightness at spot-sampled locations. Data are shown as the BCET relative brightness, i.e. represented as a value between 0 and 255. Solid lines show mean brightness for each stratigraphic unit, averaged across all fans (*n* gives the number of spot locations). Shading shows ±1 σ variability between all sampling spots. As surfaces get older, peak brightness shifts to SWIR bands (longer wavelengths), and this is observed for burned and unburned surfaces.

Fig. 4. Average spectral profiles from Fig. 3 for (A) unburned fan surfaces and (B) burned fan surfaces, normalised to band 2 (blue light). Relative brightness in bands 3-7 increases with surface age, with band 6 showing the greatest sensitivity.

Fig. 5. (A) Brightness ratio of band 6 (SWIR 1)/band 2 (blue) for each alluvial fan surface (open circles) and averaged for each stratigraphic unit (stars). Burned and unburned sampling sites are shown in red and black, respectively. There is a gradual increase in the brightness ratio with age, in agreement with Fig. 4. The stratigraphic averages are fitted with a power law regression, which predicts a starting ratio of 0.5-0.6 (when age = 0 ka), has an exponent of 0.16-0.19 and describes the data well (R^2 = 0.96-0.99). The regression parameters are identical within uncertainty if fitted to the individual fan surfaces, and R^2 decreases to 0.86 (non-burned surfaces) and 0.90 (burned surfaces). (B) The same data plotted in log-log form; the brightness ratio is a good predictor of fan surface age with the greatest sensitivity between 10-100 ka.

Fig. 6. Visible-infrared reflectance spectra for (A) 4 surface gravel samples from the Owens Valley fans. The inset panel shows the area of the (shaded) 2.2 μm absorption feature (associated with illite abundance) plotted against sample age. (B) reference minerals after Clark et al. (2007). The wavelength windows of Landsat 8 bands 1-7 are shown for comparison.

Fig. 7. Clay fraction XRD results for the Q4 and Q2b surface samples. Only low angles are displayed to focus on clay absorption features. The main peaks are associated with illite and microcline. A broad kaolinite peak appears in the Q2b sample at ~12 °, which is absent from the Q4 sample. There are also small peaks associated with chlorite. No peaks were observed associated with any other clay minerals.

Fig. 8. Oblique view of the George Creek and South Bairs Creek fans taken from Google Earth, showing (A) aerial imagery and (B) a Landsat 8 642 (RGB) false colour composite with distinct fan surfaces outlined in white. *SSNFFZ* = Southern Sierra Nevada Frontal Fault Zone.

For scale, the distance between the two major streams where they cross the SSNFFZ is ~3 km.

Fig. 9. (A) Comparison of predicted fan surface ages using the relationship in Fig. 5 for unburned surfaces, with the actual fan surface ages. (B) Plot of the error between the predicted and actual fan surface ages, compared with actual fan surface age. (C) Normalised frequency distributions of the error on fan surface age (predicted using the relationship in Fig. 5) compared with the actual fan surface ages.

Fig. 10. (A) Landsat-8 false colour composite (642 RGB, date: 14th February 2013) locating the Backthrust Canyon and Moonlight Canyon alluvial fans in Death Valley, California. BCET brightness was obtained for each Landsat-8 band for the modern fan surfaces (green and blue spots), and abandoned fan surfaces (yellow and red spots) dated to 70 ka (+22/-20 ka) by Frankel et al. (2007b) using ^{10}Be cosmogenic nuclides. (B) The band 6/band 2 ratio is calculated for each fan surface, and plotted alongside the data for unburned surfaces in Owens Valley (grey symbols and regression, see Fig. 5). The inset panel shows the BCET brightness across bands for each surface.